PHYSICAL REVIEW E **90**, 012107 (2014)

Nonequilibrium ensemble inequivalence and large deviations of the density in the ABC model

O. Cohen and D. Mukamel
Department of Physics of Complex Systems, Weizmann Institute of Science, Rehovot 7610001, Israel
(Received 19 March 2014; published 7 July 2014)

We consider the one-dimensional driven ABC model under particle-conserving and particle-nonconserving processes. Two limiting cases are studied: (a) The rates of the nonconserving processes are vanishingly slow compared with the conserving processes in the thermodynamic limit and (b) the two rates are comparable. For case (a) we provide a detailed analysis of the phase diagram and the large deviations function of the overall density, $\mathcal{G}(r)$. The phase diagram of the nonconserving model, derived from $\mathcal{G}(r)$, is found to be different from the conserving one. This difference, which stems from the nonconvexity of $\mathcal{G}(r)$, is analogous to ensemble inequivalence found in equilibrium systems with long-range interactions. An outline of the analysis of case (a) was given in an earlier letter. For case (b) we show that, unlike the conserving model, the nonconserving model exhibits a moving density profile in the steady state with a velocity that remains finite in the thermodynamic limit. Moreover, in contrast with case (a), the critical lines of the conserving and nonconserving models do not coincide. These are new features which are present only when the rates of the conserving and nonconserving processes are comparable. In addition, we analyze $\mathcal{G}(r)$ in case (b) using macroscopic fluctuations theory. Much of the derivation presented in this paper is applicable to any driven-diffusive system coupled to an external particle bath via a slow dynamics.

DOI: 10.1103/PhysRevE.90.012107 PACS number(s): 05.20.Gg, 05.50.+q, 05.70.Ln, 64.60.Cn

I. INTRODUCTION

Systems that are driven out of equilibrium by an external field, such as temperature gradient or electric field, exhibit in many cases long-range correlations in their steady states, even when their dynamics is strictly local. This has been demonstrated in numerous studies both for specific models and in more generic settings [1–7]. Studying generic steady-state features that result from these long-range correlations would be of great interest. A useful insight into this behavior may be gained by comparing it to that of an equilibrium system, where long-range correlations appear either in systems with short-range interactions at criticality or in systems with explicit long-range interactions. The latter type bears more similarity to *driven systems*, as in both cases the long-range correlations appear generically, i.e., also away from any phase transition points.

Equilibrium systems with long-range interactions are those where the two body potential decays at large distance, R, as $1/R^{d+\sigma}$, with $-d \leqslant \sigma \leqslant 0$ in d dimensions. One consequence of this long-range decay is nonadditivity, whereby the energy does not increase linearly with the system's size. Nonadditivity may cause various ensembles of the same long-range interacting system to exhibit different phase diagrams, as has been shown in numerous studies [8–21]. This occurs, for instance, when the microcanonical entropy is not a convex function of the energy for a certain range of energies, leading to negative specific heat in the microcanonical ensemble. This is in contrast with the canonical ensemble, where the entropy is inherently convex and the specific heat is non-negative. Similar effects can be found when comparing the canonical and the grand-canonical ensembles [22–24].

In a recent letter [25] we demonstrated that a phenomenon similar to ensemble inequivalence exists in a specific driven system, known as the ABC model [26,27]. The ABC model is defined on a one-dimensional lattice of length L, where each site is occupied by one particle of type A, B, or C. The model evolves by sequential updates whereby particles on randomly chosen neighboring sites are exchanged with the following rates:

$$AB \underset{1}{\overset{q}{\rightleftarrows}} BA, \quad BC \underset{1}{\overset{q}{\rightleftarrows}} CB, \quad CA \underset{1}{\overset{q}{\rightleftarrows}} AC. \tag{1}$$

The ABC model is often studied in the limit of weak asymmetry where the asymmetry in the rates scales with the size of the system, L, as $q = \exp(-\beta/L)$ [28]. With this scaling the model undergoes a transition between a phase where the particles are homogenously distributed in the system and a phase where the three species phase separate into three macroscopic domains [28]. The value of β where the transition occurs is a function of the average densities of particles, defined as $r_\alpha \equiv N_\alpha/L$ for $\alpha = A, B, C$, where N_α is the overall number of particles of type α. A unique property of the ABC model is that when the number of particles of the three species are equal, $N_A = N_B = N_C$, the model obeys detailed balance with respect to an effective Hamiltonian with long-range interactions. This special equilibrium point provides an analytical framework for investigating the mechanism behind long-range correlations in driven systems.

The ABC model has been generalized to include particle-non-conserving process in [24,29]. In this generalized model sites can also be occupied by inert vacancies, denoted by 0, whose dynamics is defined as

$$A0 \underset{1}{\overset{1}{\rightleftarrows}} 0A, \quad B0 \underset{1}{\overset{1}{\rightleftarrows}} 0B, \quad C0 \underset{1}{\overset{1}{\rightleftarrows}} 0C. \tag{2}$$

In addition, triplets of particles can evaporate and condense with the rates

$$ABC \underset{p}{\overset{p\, e^{-3\beta\mu}}{\rightleftarrows}} 000, \tag{3}$$

where p is a rate parameter and μ plays the role of the chemical potential. Studies of this model in the *equal-densities*

regime revealed inequivalence between the phase diagram of a *conserving model*, defined by rules (1)–(2), and that of a *nonconserving model*, defined by rules (1)–(3). The two models correspond to the canonical and grand-canonical ensembles of the ABC Hamiltonian, respectively. The generalized ABC model has then been analyzed for nonequal densities, where an effective Hamiltonian cannot be defined [25] and was demonstrated to exhibit a similar inequivalence between the conserving and nonconserving phase diagrams.

In this paper we generalize the analysis of [25] and present a detailed study of the ABC model with particles nonconserving processes. In the first part of the paper we study the nonconserving ABC model in the limit where the ratio between the time scale of the nonconserving dynamics, given by $1/p$, and that of the conserving dynamics, given by $\tau \sim L^2$, vanishes in the thermodynamic limit. We thus consider $p \sim L^{-\gamma}$ with $\gamma > 2$. In this limit, we are able to compute the large deviations function (rate function) of the overall density of particles, $\mathcal{G}(r)$ with $r \equiv (N_A + N_B + N_C)/L$, and derive from it the exact phase diagram of the nonconserving model. This is done by analyzing the dynamics of r, which can be effectively represented as a one-dimensional random walk in a potential. The form of the potential is derived from the coarse-grained density profile of the ABC model, computed in [30]. The nonconserving phase diagram for nonequal densities, derived from $\mathcal{G}(r)$, is similar to that obtained for equal densities, excluding several features discussed below. As in the equal-densities case and similarly to equilibrium systems with long-range interactions, the conserving and the nonconserving models undergo the same second order transition and become inequivalent when the transition in the nonconserving model turns into first order. This suggests that a phenomenon similar to ensemble inequivalence, which characterizes many long-range interacting systems, may be found in other driven-diffusive systems that exhibit long-range correlations.

In the second part of the paper we study the nonconserving ABC model in the limit where the rates of the conserving and nonconserving dynamics are comparable, namely for $p = \phi L^{-2}$ with ϕ being an arbitrary parameter. In this case the conserving and the nonconserving models exhibit different critical lines and steady-state density profiles. Such inequivalence is expected to be found only in nonequilibrium systems. Interestingly, the density profile of the nonconserving model is found to exhibit a drift velocity in its ordered phase. The velocity remains finite even in the thermodynamic limit and can be computed exactly along the critical line. This is in contrast with the conserving ABC model, where for $r = 1$ the drift velocity has been shown to vanish as $1/L$ [31] and has been excluded in the thermodynamic limit [32]. This can be shown to be valid also for the conserving model with $r < 1$ using the mapping between the $r = 1$ and $r < 1$ cases, discussed below.

The probability of a rare number of particles in the nonconserving model, $P(r) \sim e^{L\mathcal{G}(r)}$, can be studied for $p = \phi L^{-2}$ using the macroscopic fluctuation theory [33–38]. By analyzing the instanton path leading to a rare value of r, we derive an expansion of $\mathcal{G}(r)$ in powers of ϕ for $\phi \ll 1$. The lowest order in this expansion is identical to the expression obtained for $p \sim L^{-\gamma}$ and $\gamma > 2$. This fact serves as a proof that $\gamma > 2$ is indeed the limit where the conserving and nonconserving time scales are well separated. In the homogenous phase the corrections to $\mathcal{G}(r)$ vanish for all ϕ, yielding the same expression for $\gamma > 2$ and $\gamma = 2$. This conclusion is expected to remain valid for a large class of driven-diffusive systems that exhibit a homogenous phase.

This paper is organized as follows. We first provide a brief review of the ABC model and previous studies of the equal-densities regime in Sec. II. We study the phase diagram of the nonconserving ABC model for nonequal densities and in the limit of very slow nonconserving dynamics ($\gamma > 2$) in Sec. III. In Sec. IV we study the model in the limit where the conserving and the nonconserving dynamics occur on comparable time scales ($\gamma = 2$). Concluding remarks and outlook are given in Sec. V.

II. THE ABC MODEL WITH EQUAL DENSITIES

The standard ABC model is defined by the dynamical rules in Eq. (1). For $q = 1$, this dynamics yields a homogeneous steady state, in which the particles are distributed uniformly on the lattice. On the other hand, for $q \neq 1$ the model relaxes in the $L \to \infty$ limit to a state where the particles phase separate into three domains. The domains are arranged clockwise for $q < 1$, i.e., $AA,\ldots,ABB,\ldots,BCC,\ldots,C$, and counterclockwise for $q > 1$. Throughout this paper we assume $q < 1$. The case of $q > 1$ is obtained by considering a system with a driving field $q' = 1/q < 1$ and exchanging, say, the B and C labels.

As a result of the dynamical asymmetry, the model exhibits in general nonvanishing steady-state currents of particles. The current of particles of a given species is proportional to the rate at which the particles of this species perform a full clockwise trip minus the rate of the counterclockwise trip, yielding

$$J_\alpha \sim q^{N_{\alpha+1}} - q^{N_{\alpha+2}}, \tag{4}$$

where α runs cyclically over A, B, C and N_α denotes the overall number of particles of species α. In the *equal-densities case*, where $N_A = N_B = N_C = L/3$, the currents vanish and the dynamics can be shown to obey detailed balance with respect to an effective long-range Hamiltonian given by

$$\mathcal{H}(\boldsymbol{\zeta}) = \sum_{i=1}^{L}\sum_{k=1}^{L-1}\frac{k}{L}\left(A_i B_{i+k} + B_i C_{i+k} + C_i A_{i+k}\right). \tag{5}$$

Here $\boldsymbol{\zeta} = \{\zeta_i\}_{i=1}^{L}$ denotes a microstate of the system such that $\zeta_i = A$, B, or C, and

$$X_i = \begin{cases} 1 & \zeta_i = X \\ 0 & \zeta_i \neq X \end{cases} \quad \text{for } X = A, B, C. \tag{6}$$

The steady-state probability measure is given in terms of the Hamiltonian by $P(\boldsymbol{\zeta}) \propto q^{\mathcal{H}(\boldsymbol{\zeta})}$ [26].

The Hamiltonian in Eq. (5) can also be written in a more instructive form as

$$\mathcal{H}(\boldsymbol{\zeta}) = \frac{1}{2}\sum_{i=1}^{L-1}\sum_{k=1}^{i-1}[A_i(B_k - C_k) + B_i(C_k - A_k) + C_i(A_k - B_k)], \tag{7}$$

where every particle appears to be positioned in a potential well created by the particles of the two other species, as illustrated

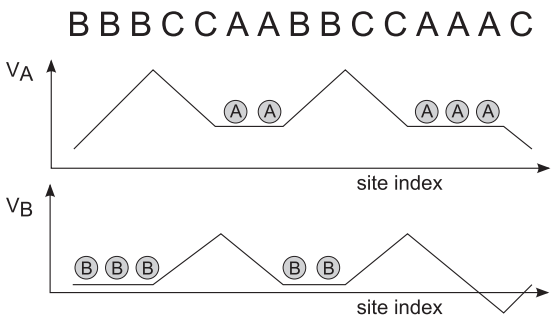

FIG. 1. Effective potential exerted on the A particles, $V_{A,i} = \sum_{k=1}^{i-1} B_k - C_k$, and on the B particles, $V_{B,i} = \sum_{k=1}^{i-1} C_k - A_k$, drawn for a specific configuration of a system of size $L = 15$. The configuration itself is written above the two figures.

in Fig. 1 for a specific configuration. The factor $1/2$ corrects for the double counting of the interactions. Clearly, this potential picture breaks down for nonequal densities, where the system relaxes to a nonequilibrium steady state.

We consider in this paper the limit of weak asymmetry, where $q \to 1$ in the $L \to \infty$ limit as $q = \exp(-\beta/L)$, with β being a positive parameter [28]. As a result of this scaling, the energy and the entropy of the system become comparable in size in the thermodynamic limit. The parameter β which sets the ratio between the energy and the entropy can be regarded as the inverse temperature of the system. This rescaling is similar to the Kac's prescription often employed in systems with long-range interactions [39]. For equal densities, the model exhibits in the $L \to \infty$ limit a second order phase transition at $\beta = \beta_c = 2\pi\sqrt{3}$ between a homogeneous state, where entropy dominates, and an ordered state which is dominated by the energy term [28].

Ensemble inequivalence can be studied in the ABC model by comparing its canonical and grand-canonical phase diagrams. To this end we consider a generalization of the original model where sites may also be vacant [24]. In this case, particles can hop into and out of vacant sites, denoted by 0, with symmetric rates given by Eq. (2). The number of vacancies is $N_0 \equiv L - N$, where $N \equiv N_A + N_B + N_C \leqslant L$. We refer to this model, which consists of rules (1) and (2), as the *conserving ABC model*.

The steady-state properties of the conserving model can be derived by mapping it onto the standard ABC model in which $N = L$. This is a many-to-one mapping which consists of removing the vacancies in a microconfiguration, $\boldsymbol{\zeta}$, of the generalized model of length L, yielding a configuration of length N, denoted by $\mathbf{f}(\boldsymbol{\zeta})$. Using the fact that the vacancies evolve by a simple diffusion (2) and are thus homogenously distributed in the steady state, it can easily be shown that the steady-state measure of the generalized model is given by

$$P_L(\boldsymbol{\zeta}; N) = P_N(\mathbf{f}(\boldsymbol{\zeta}); N) \Big/ \binom{L}{N}, \tag{8}$$

where $P_L(\boldsymbol{\zeta}; N)$ denotes the steady-state measure of the ABC model of size L and with N particles. For equal-densities the latter is given in the standard ABC model ($L = N$) by $P_N(\boldsymbol{\zeta}; N) \propto q^{\mathcal{H}(\boldsymbol{\zeta})}$. By defining an effective inverse temperature β' as $q = \exp(\beta/L) = \exp(\beta r/N) \equiv \exp(\beta'/N)$, where $r = N/L$, we conclude that the N-size system has an effective inverse temperature $\beta' = \beta r$. Similarly, the average densities of the N-size system are $r'_\alpha = r_\alpha/r$ for $\alpha = A, B, C$. Using this mapping the critical point of the equal-densities standard ABC model [28], $\beta_c = 2\pi\sqrt{3}$, is mapped onto a critical line in the equal-densities conserving model, given by

$$\beta_c = 2\pi\sqrt{3}/r. \tag{9}$$

The *nonconserving ABC model* is defined by allowing for evaporation and deposition of particles, performed in triplets of neighboring particles according to Eq. (3). For $N_A = N_B = N_C$, this specific type of nonconserving process can be shown to maintain detailed balance with respect to the Hamiltonian

$$\mathcal{H}_{GC}(\boldsymbol{\zeta}) = \mathcal{H}(\boldsymbol{\zeta}) - \mu N L, \tag{10}$$

where $\mathcal{H}(\boldsymbol{\zeta})$ is defined in Eq. (7) [40]. This allows one to study the nonconserving model using equilibrium techniques. It has been shown in [24] that for equal densities the nonconserving model also exhibits a second order transition line at $\beta_c = 2\pi\sqrt{3}/r$ for $r \geqslant r_{TCP}$, where $r_{TCP} = 1/3$ is the tricritical point. Below this point, for $r < r_{TCP}$, the nonconserving model exhibits a first order transition, whereas the transition in the conserving model remains second order. The resulting phase diagrams of the conserving and nonconserving models, which have been derived for equal densities in [29], are plotted in Fig. 2. The generalization of this phase diagram to arbitrary densities, where one cannot use the Hamiltonian in Eq. (5), is discussed in the next section.

In order to compare the two ensembles, the canonical phase diagram is plotted in Fig. 2 as a function of the chemical potential, which is defined as

$$\mu(r) = d\mathcal{F}(r)/dr, \tag{11}$$

where $\mathcal{F}(r)$ is the free energy of the conserving ABC model. For equal densities, the latter has been computed in [29] in the $L \gg 1$ limit based on a continuum description of the model as

$$\mathcal{F}(r) = E[\boldsymbol{\rho}^\star(x,r)] - \frac{1}{\beta} S[\boldsymbol{\rho}^\star(x,r)].$$

Here $\boldsymbol{\rho}^\star(x,r) \equiv [\rho_A^\star(x,r), \rho_B^\star(x,r), \rho_C^\star(x,r)]$ is the steady-state profile of the conserving model with particle density r, whose form is discussed in Sec. III B. The functionals S and E correspond to the entropy and the energy per particle for a given density profile, respectively. The former is derived from combinatorial considerations, yielding $S[\boldsymbol{\rho}] = -\sum_\alpha \int_0^1 dx \rho_\alpha(x) \ln \rho_\alpha(x) - \int_0^1 dx \rho_0(x) \ln \rho_0(x)$, and the latter is derived from the Hamiltonian in Eq. (7), yielding $E[\boldsymbol{\rho}] = \frac{1}{2}\sum_\alpha \int_0^1 dx \int_0^x dy \rho_\alpha(x)[\rho_{\alpha+1}(y) - \rho_{\alpha+2}(y)]$. Here and below α runs cyclically over A, B, and C and $\rho_0(x) \equiv 1 - \sum_\alpha \rho_\alpha(x)$.

III. ABC MODEL WITH NONEQUAL DENSITIES AND VANISHINGLY SLOW NONCONSERVING DYNAMICS ($p \sim L^{-\gamma}, \gamma > 2$)

In this section we study the steady-state properties of the ABC model for arbitrary densities both under conserving dynamics and nonconserving dynamics whose rate, p, is vanishingly slower than the diffusive dynamics for $L \to \infty$.

For arbitrary densities, in the absence of a Hamiltonian which describes the steady-state measure of the model, the

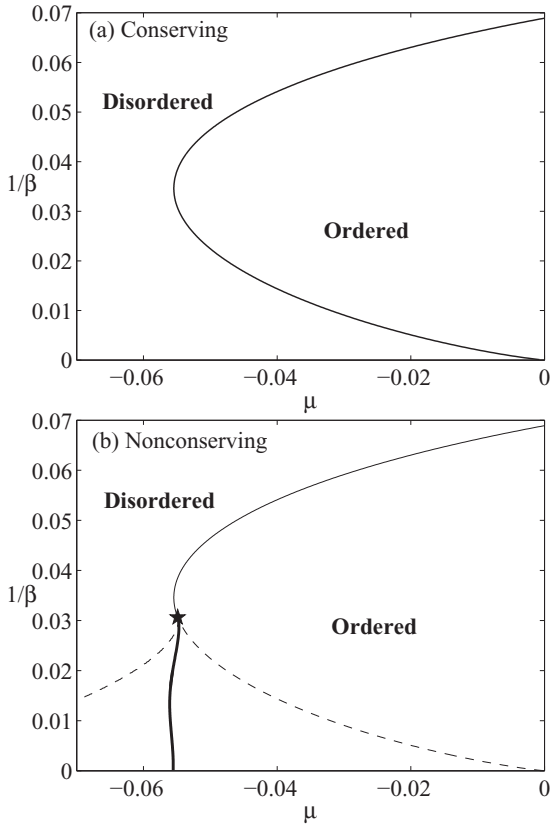

FIG. 2. Phase diagram of the conserving (a) and nonconserving (b) ABC models with equal densities, $N_A = N_B = N_C$, plotted in the $(\mu, 1/\beta)$ plane. The two diagrams show the same second order transition line (thin solid line). In the nonconserving model the transition line turns into a first order (thick solid line) at a tricritical point ($\star$). The boundaries of the coexistence region, where both the homogenous and the ordered profiles are locally stable, are denoted in the nonconserving model by dashed lines.

analysis of the model is based on a continuum description which is valid, in general, for diffusive systems such as the weakly asymmetric ABC model. In the continuum limit the probability of a microconfiguration $\boldsymbol{\zeta}(t)$ is approximated by a smooth density profile defined as

$$\Pr[\zeta_i(t) = \alpha] \simeq \rho_\alpha(i/L, t/L^2) \tag{12}$$

for $\alpha = A, B, C$. The evolution of the coarse-grained density profile, $\rho_\alpha(x,\tau)$, is given in the conserving model by the following hydrodynamic equation [28]:

$$\partial_\tau \rho_\alpha = \beta \partial_x \left[\rho_\alpha \left(\rho_{\alpha+1} - \rho_{\alpha+2}\right)\right] + \partial_x^2 \rho_\alpha. \tag{13}$$

The density profile is periodic, $\rho_\alpha(x+1,\tau) = \rho_\alpha(x,\tau)$, and due to exclusion it obeys $\rho_0(x,\tau) = 1 - \sum_\alpha \rho_\alpha(x,\tau) \leqslant 1$. Equation (13) has been shown to be exact in the $L \to \infty$ limit for equal densities and $r = 1$ [28,41] and has been argued to remain valid even for arbitrary average densities [32,41]. The mapping discussed in Sec. II between the $r = 1$ and the $r < 1$ cases implies that the steady-state properties resulting from the study of Eq. (13) for $r = 1$ can be mapped onto the $r < 1$ case.

Within the hydrodynamic framework, the addition of the nonconserving dynamics in (3) yields

$$\begin{aligned}\partial_\tau \rho_\alpha = {} & \beta \partial_x \left[\rho_\alpha \left(\rho_{\alpha+1} - \rho_{\alpha+2}\right)\right] + \partial_x^2 \rho_\alpha \\ & + L^2 p \left(\rho_0^3 - e^{-3\beta\mu} \rho_A \rho_B \rho_C\right),\end{aligned} \tag{14}$$

where the L^2 factor of the nonconserving term is due to the rescaling of time, $\tau = t/L^2$, and of space, $x = i/L$. Using the same reasoning discussed in [32] for the derivation of Eq. (13), the local-equilibrium approximation can be shown to be valid when the rate of the nonconserving dynamics is vanishingly slower than the diffusive dynamics, i.e., for $p \sim L^{-\gamma}$ and $\gamma > 2$. This implies that Eq. (14) is valid for $\gamma > 2$. In Sec. IV B, Eq. (14) is shown to be valid also for $\gamma = 2$, by demonstrating that it corresponds to the extremum of the large deviation function of $\boldsymbol{\rho}(x,\tau)$.

In the following sections we analyze the phase diagram of the nonconserving model for $\gamma > 2$, first in Sec. III A by expanding Eq. (14) around its homogenous solution and then in Sec. III B by computing $\mathcal{G}(r)$ from the steady-state solution of Eq. (13).

A. Critical expansion of the ABC model

1. Conserving dynamics

We consider first the conserving ABC model, described by Eq. (13). In order to find the critical point of the model one can expand its density profile around the homogenous solution $\rho_\alpha(x) = r_\alpha$. Following the approach presented in [42] for the equal-densities case, we expand the profile in terms of Fourier modes in x space and in terms of the eigenvectors of the matrix $\mathcal{T}_{\alpha,\alpha'} \equiv \delta_{\alpha+1,\alpha'} - \delta_{\alpha+2,\alpha'}$ in the species space. The density profile can thus be written as

$$\begin{aligned}\begin{pmatrix}\rho_A \\ \rho_B \\ \rho_C\end{pmatrix} = \sum_{m=-\infty}^{\infty} e^{2\pi i m x} \Bigg[& \frac{a_m(\tau)}{\sqrt{3}} \begin{pmatrix}1 \\ e^{-2\pi i/3} \\ e^{2\pi i/3}\end{pmatrix} \\ & + \frac{a^\star_{-m}(\tau)}{\sqrt{3}} \begin{pmatrix}1 \\ e^{2\pi i/3} \\ e^{-2\pi i/3}\end{pmatrix} + \frac{b_m(\tau)}{3} \begin{pmatrix}1 \\ 1 \\ 1\end{pmatrix}\Bigg].\end{aligned} \tag{15}$$

There are several points to note about this expansion. Integrating Eq. (15) over x yields

$$\begin{pmatrix}r_A \\ r_B \\ r_C\end{pmatrix} = \frac{b_0}{3} \begin{pmatrix}1 \\ 1 \\ 1\end{pmatrix} + \frac{2}{\sqrt{3}} |a_0| \begin{pmatrix}\cos\theta \\ \cos\left(\theta - \frac{2\pi}{3}\right) \\ \cos\left(\theta + \frac{2\pi}{3}\right)\end{pmatrix}, \tag{16}$$

where $\theta = \arg(a_0)$. Summing Eq. (16) over $\alpha = A, B, C$ yields $b_0 = r_A + r_B + r_C = r$, which implies that b_0 represents the average density. On the other hand, a_0 sets the deviation of r_A, r_B and r_C from the equal-densities point. Similarly for $m \neq 0$, the values of b_m set the profile of the vacancies while a_m set the local deviation from equal densities. One reason to choose the eigenvectors of $\mathcal{T}$ is because they decompose the deviations from equal densities in a symmetric way that does not prefer any specific species.

Inserting the above expansion (15) into Eq. (13) we find that the evolution of a_m and b_m is decoupled and given by

$$\partial_\tau a_m = -\frac{2\pi m}{3}\left[(6\pi m - \sqrt{3}\beta r)a_m + 3\beta \sum_{m'=-\infty}^{\infty} a^\star_{-m-m'} a^\star_{m'}\right], \tag{17}$$

$$\partial_\tau b_m = -4\pi^2 m^2 b_m. \tag{18}$$

The latter equation reflects the fact that the inert vacancies perform an unbiased diffusion and hence their steady-state profile is flat, $\rho_0(x,\infty) = 1 - r$, or equivalently $b_m(\infty) = 0$ for $m \neq 0$.

In order to find the critical line one has to consider small perturbations around the homogenous profile by taking $a_m \ll 1$. For nonequal densities, where $a_0 \neq 0$, the nonlinear term in Eq. (17) contributes to the lowest order equation of a_m. To lowest order in a_m one finds a linear dependence between a_m and $a^\star_{-m}$ given by

$$\begin{pmatrix} \partial_\tau a_m \\ \partial_\tau a^\star_{-m} \end{pmatrix} = -\frac{2\pi m}{3} A_m \begin{pmatrix} a_m \\ a^\star_{-m} \end{pmatrix} + O\left(a_m^2\right),$$

where

$$A_m \equiv \begin{pmatrix} 6\pi m - \sqrt{3}\beta r & 6\beta a_0^\star \\ -6\beta a_0 & 6\pi m + \sqrt{3}\beta r \end{pmatrix}. \tag{19}$$

The critical point of the model is obtained when the highest of the eigenvalues of $-\frac{2\pi m}{3} A_m$ vanishes and as a result the amplitude of the corresponding eigenvector becomes unstable. Out of all the eigenvalues of $-\frac{2\pi m}{3} A_m$, given by

$$\epsilon_\pm^{(m)} = -\frac{2\pi m}{3}[6m\pi \mp \beta\sqrt{3(r^2 - 12|a_0|^2)}], \tag{20}$$

the highest one is $\epsilon_+^{(1)}$ and it vanishes at

$$\beta = \beta_c \equiv \frac{2\pi\sqrt{3}}{\sqrt{r^2 - 12|a_0|^2}}. \tag{21}$$

Equation (21) can be written in terms of r_α by taking the square of Eq. (16), yielding

$$|a_0|^2 = \frac{1}{2}\sum_{\alpha=A,B,C}(r_\alpha - r/3)^2. \tag{22}$$

As expected, the critical line in Eq. (21) coincides with the result for $r = 1$ obtained in [28].

For $\beta = \beta_c(1+\delta)$ with $\delta \ll 1$, the existence of an ordered profile whose amplitude vanishes with δ corresponds to a continuous transition at $\beta = \beta_c$. To leading order in δ, only the eigenvector corresponding to $\epsilon_+^{(1)}$ is excited and the other Fourier modes are driven by it through the nonlinear terms in Eq. (17). Denoting the amplitude of this eigenvector by φ, one can expand Eq. (17) in powers of φ, yielding

$$\partial_\tau \varphi = 4\pi^2\delta\varphi + G_4^c(r,a_0)\varphi|\varphi|^2 + G_6^c(r,a_0)\varphi|\varphi|^4 + O(\varphi^7), \tag{23}$$

where the superscript c refers to the conserving dynamics. In Appendix A, the form of $G_i^c(r,a_0)$ is obtained explicitly for $i = 4$ and studied numerically for $i = 6$. The case where $G_4^c(r,a_0) > 0$ yields an ordered profile whose amplitude vanishes as $\delta^{1/2}$, whereas for $G_4^c(r,a_0) < 0$ the steady-state profile has a finite amplitude. One can thus identify the point where $G_4^c(r,a_0) = 0$ and $\beta = \beta_c$ as the tricritical point of the model, below which, for $G_4^c(r,a_0) < 0$, the critical line is preempted by a first order transition. The condition of $\beta = \beta_c$ and $G_4^c(r,a_0) < 0$ is shown in Appendix A to correspond to

$$2\left(r_A^3 + r_B^3 + r_C^3\right) > (r_A + r_B + r_C)\left(r_A^2 + r_B^2 + r_C^2\right). \tag{24}$$

This condition coincides with that obtained for $r = 1$ in [28].

The critical line in Eq. (21) and the above tricritical point, where $\beta = \beta_c$ and $G_4^c(r,a_0) = 0$, are plotted for a specific value of a_0 in Fig. 3(a). For comparison with the nonconserving model the conserving phase diagram is plotted as a function of the parameter μ. This parameter is obtained by inverting the relation between r and μ in the nonconserving model, which is computed in the next section. In order to draw the first order transition line in the conserving model, one has to know the large deviations function of the density profile, which has been derived only in the limit of $a_0 \ll 1$ [28] or $\beta \gg 1$ [43]. Without the probability of each stationary profile, one cannot distinguish between stable and metastable states, as necessary for locating first order transition points. However, using the steady-state density profile of the conserving model, discussed in Sec. III B, one can draw the stability limits around the first order transition line, denoted by dashed lines in Fig. 3(a).

2. Slow nonconserving dynamics

A similar critical expansion can be carried out in the nonconserving model. The main difference between the two expansions is the additional term in the equation of b_m due to the nonconserving dynamics. In the limit of $p \sim L^{-\gamma}$ and $\gamma > 2$ this additional term is negligible with respect to the diffusive term in Eq. (18) for $m \neq 0$. This implies that the profile of the vacancies remains flat. The nonconserving term is of leading order only for b_0, whose equation can be obtained by summing Eq. (14) over $\alpha = A,B,C$ and integrating the result over x, yielding

$$\begin{aligned}\partial_\tau b_0 &= 3pL^2\int_0^1 dx\left(\rho_0^3 - e^{-3\beta\mu}\rho_A\rho_B\rho_C\right) \\ &= 3pL^2\left\{(1-b_0)^3 - e^{-3\beta\mu}\left[\frac{b_0^3}{27} - \frac{b_0}{3}\sum_{m_1} a_{m_1}a^\star_{m_1}\right.\right. \\ &\quad \left.\left. + \frac{1}{3\sqrt{3}}\sum_{m_1,m_2}(a_{m_1}a_{m_2}a_{-m_1-m_2} + \text{c.c.})\right]\right\}. \end{aligned} \tag{25}$$

In the expansion of b_0 around its average value it is useful to consider fluctuations in the overall density, defined as $\delta r \equiv b_0 - r$. In the nonconserving model, r denotes the overall density in the homogenous phase, obtained by setting $a_m = 0$ for $m \neq 0$ in Eq. (25), which yields

$$e^{-3\beta\mu} = \frac{27(1-r)^3}{r(r^2 - 9|a_0|^2)}. \tag{26}$$

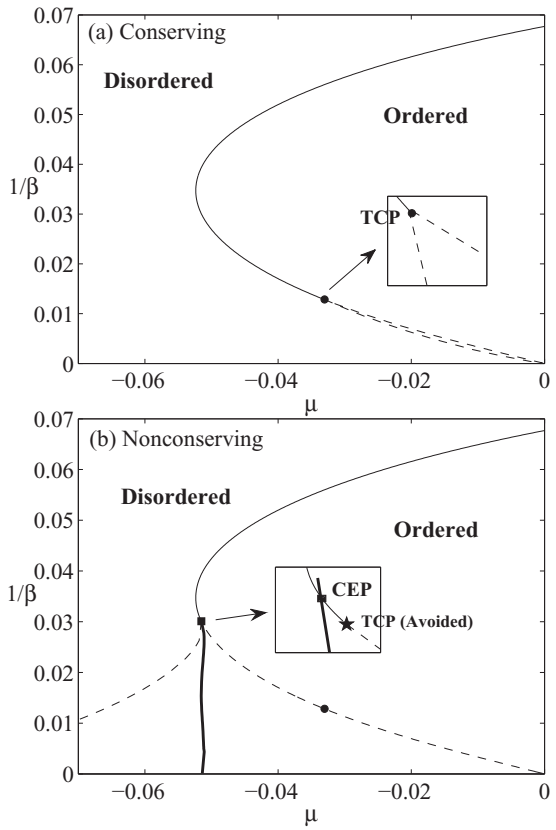

FIG. 3. Phase diagram of the conserving (a) and nonconserving (b) ABC models for in two-equal-densities case, $r_A = r_B = r/3 - 0.01$ and $r_C = r/3 + 0.02$, or, equivalently, $a_0 = 0.01\sqrt{3}e^{i\pi/3}$, plotted in the $(\mu, 1/\beta)$ plane. The two diagrams show the same second order transition line (thin solid line). In the conserving model the transition line turns at the tricritical point (•) into a first order transition line, which cannot be computed without knowing the full large deviations function of the ABC model. In the nonconserving model the transition line turns into first order (thick solid line) at a critical end point (■), which appears at a higher value of $1/\beta$ than the tricritical point (⋆). Both diagrams are supplemented by an illustration of the region where the first and second order transition lines meet. The boundaries of the coexistence regions, where both the homogenous and the ordered profiles are locally stable, are denoted by dashed lines.

The fluctuations in b_0 modify the evolution of a_m, which is given by

$$\partial_\tau a_m = -\frac{2\pi m}{3}\left[(6\pi m - \sqrt{3}\beta r)a_m - \sqrt{3}\beta\delta r a_m + 3\beta\sum_{m'=-\infty}^{\infty} a^\star_{-m-m'}a^\star_{m'}\right]. \quad (27)$$

By inserting the definition $b_0 = r + \delta r$ into Eq. (25) and expanding it in leading order in δr, one obtains that slightly below the critical line $\delta r \sim |a_m|^2$. This implies that δr does not affect the linear stability of a_m in Eq. (27), leading to a nonconserving critical line that is identical to the conserving line in Eq. (21). The effect of δr appears only in higher order critical points. As in the conserving model, equation Eq. (27) is expanded in Appendix A in powers of the amplitude of the first excited eigenvector, φ, yielding

$$\partial_\tau\varphi = 4\pi^2\delta\varphi + G_4^{nc}(r,a_0)\varphi|\varphi|^2 + G_6^{nc}(r,a_0)\varphi|\varphi|^4 + O(\varphi^7). \quad (28)$$

In this expansion we find that $G_4^{nc}(r,a_0) \neq G_4^{c}(r,a_0)$, leading to a different tricritical points in the conserving and nonconserving models.

In Appendix A we also study numerically $G_6^c(r,a_0)$ and $G_6^{nc}(r,a_0)$. In general, if this coefficient is positive at the point where $\beta = \beta_c$ and $G_4 = 0$, the model exhibits a tricritical point connecting the second order and first order transition lines. This is the case in the conserving model, plotted in Fig. 3(a), and in the nonconserving model only for relatively high values of $|a_0|$. Figure 3(b) shows the opposite case, where $G_6^{nc} < 0$, which occurs in the nonconserving model for $|a_0| \neq 0$ but relatively small. In this case the point where $\beta = \beta_c$ and $G_4^{nc} = 0$ [TCP in Fig. 3(b)] is preempted by a critical end point [CEP in Fig. 3(b)], which connects the second and the first order transition lines. The first order transition line continues into the ordered phase, where it signifies a transition between a low density and high density ordered phases. The first order transition line in this figure is derived in the next section. Remarkably, in the equal-densities case the second and first order transition lines are connected by a fourth order critical point where $\beta = \beta_c$, $G_4^{nc} = G_6^{nc} = 0$, and $G_8^{nc} > 0$ [29]. It is not yet clear whether this high order criticality is merely a coincidence or a result of an unidentified symmetry of the model.

B. Nonperturbative study of the nonconserving phase diagram

In this section we derive the first order transition line of the ABC model with slow nonconserving dynamics, shown in Fig. 3(b). The derivation is based on the exact expression for the steady-state density profile of the conserving ABC model, $\boldsymbol{\rho}^\star(x,\beta,r,a_0)$, which has been computed for $a_0 = 0, r = 1$ in [41], for $a_0 \neq 0, r = 1$ in [30], and for $a_0 \neq 0, 0 < r \leqslant 1$ in [25]. We first discuss the derivation of $\boldsymbol{\rho}^\star$ and then use it to compute the large deviations function of r.

In general, the derivation of $\boldsymbol{\rho}^\star$ is done by setting $\partial_t\rho_\alpha = 0$ in Eq. (13) (moving steady-state profiles has been excluded in [32]) and integrating over x, yielding

$$J_\alpha = -\beta\left[\rho_\alpha\left(\rho_{\alpha+1} - \rho_{\alpha+2}\right)\right] - \partial_x\rho_\alpha. \quad (29)$$

Here $\mathbf{J} \equiv (J_A, J_B, J_C)$ are the steady-state currents of particles, which obey $J_A + J_B + J_C = 0$ due to the local particle conservation. Through several additional algebraic manipulations, described in [30] for $r = 1$, the above equation can be reduced to a single ordinary differential equation, which corresponds to the motion of a particle in a quartic potential with x playing the role of time. The stationary trajectories of the particle can be written in terms of elliptic functions [30]. The stationary density profiles of Eq. (13) for $r = 1$, can then be computed from these trajectories. Using the mapping discussed in the paragraph below Eq. (9) the profile for arbitrary r can be written as

$$\boldsymbol{\rho}^\star(x,\beta,r,a_0) = r\,\boldsymbol{\rho}^\star(x,\beta r,1,a_0/r). \quad (30)$$

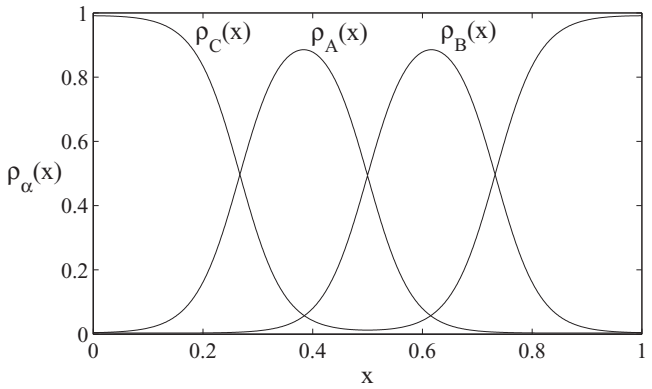

FIG. 4. The $m = 1$ ordered density profile obtained from the solution of Eq. (29) for $r_A = r_B = 7/30$ and $r_C = 16/30$ and $\beta = 25$.

For brevity, we omit from here on the dependence of $\boldsymbol{\rho}^\star$ on β and a_0 and denote the steady-state profile in Eq. (30) by $\boldsymbol{\rho}^\star(x,r)$.

According to the analysis presented in [30], one finds that for low values of β the particle has only a constant trajectory in time which corresponds to a homogenous profile. Whenever β is increased above $m\beta_c$ for $m = 1,2,\ldots$, with β_c defined in Eq. (21), the equation exhibits an additional stationary trajectory with m oscillations in the period $0 \leqslant x \leqslant 1$. An example of the corresponding profile with $m = 1$ is plotted in Fig. 4. In the equal-density case, the $m = 1$ can be shown to exhibit a lower free energy than all the $m > 1$ solutions [41]. It is therefore the only stable ordered profile observed in the thermodynamic limit. This is assumed to remain true also for arbitrary densities based on numerical evidence from Monte Carlo simulations. The function $\boldsymbol{\rho}^\star(x,r)$ therefore denotes here and below the homogenous profile for $\beta \leqslant \beta_c$ and the $m = 1$ ordered profile for $\beta > \beta_c$.

We now derive the large deviations function of r using $\boldsymbol{\rho}^\star(x,r)$ in the limit of very slow nonconserving dynamics, $p \sim L^{-\gamma}$ and $\gamma > 2$. In this limit the nonconserving term in Eq. (14) is negligible in comparison to the drift and diffusion terms. Summing Eq. (14) over $\alpha = A,B,C$ yields

$$\partial_\tau r = 3L^2 p \int_0^1 \left(\rho_0^3 - e^{-3\beta\mu}\rho_A\rho_B\rho_C\right), \tag{31}$$

where $r(\tau) = \sum_\alpha \int_0^1 dx\rho_\alpha(x,\tau)$. This implies that r evolves on a time scale of order $1/p$ (recall that $\tau = t/L^2$). The probability to observe a rare value of r can be derived by noting that on a time scale of $1/p$ the density profile is given by

$$\boldsymbol{\rho}(x,\tau) = \boldsymbol{\rho}^\star(x,r(\tau)) + O(pL^2). \tag{32}$$

This is correct even for $r(\tau)$, which is far from the steady-state value. Thus, as long as $pL^2 \ll 1$, one would expect the density profile to be given by the steady-state profile of the conserving system with overall density $r(\tau)$. As a result, the dynamics of the system can be described on this time scale as a one-dimensional master equation given by

$$\begin{aligned}\frac{1}{p}\partial_t P(r,t) = {} & w^-\left(r+\frac{3}{L}\right)P\left(r+\frac{3}{L},t\right) \\ & + w^+\left(r-\frac{3}{L}\right)P\left(r-\frac{3}{L},t\right) \\ & - P(r,t)[w^-(r)+w^+(r)].\end{aligned} \tag{33}$$

Here $P(r,t)$ is probability distribution of r, and w^-, w^+ denote the average rates of evaporation and deposition, respectively.

The evaporation rate is defined using the conserving probability measure, $P_L(\boldsymbol{\zeta}\,;N)$, as

$$\begin{aligned}w^-(r) &\equiv \frac{1}{L}e^{-3\beta\mu}\sum_{\boldsymbol{\zeta}} P_L\left(\boldsymbol{\zeta}\,;Lr\right)\sum_{i=1}^{L} A_i B_{i+1} C_{i+2} \\ &= e^{-3\beta\mu}\int_0^1 dx\rho_A^\star(x,r)\,\rho_B^\star(x,r)\rho_C^\star(x,r) + O\left(\frac{1}{L}\right),\end{aligned} \tag{34}$$

where the first index of $\zeta_{i,\alpha}$ runs cyclically over $i \in [1,L]$. The fact that the leading order contribution to the local correlation function, $A_i B_{i+1} C_{i+2}$, is given by the corresponding product of the coarse-grained density profiles is a characteristic property of diffusive systems. It is shown explicitly for the equal-densities ABC model in [28,41] and argued to be true also for arbitrary average densities in [32,41]. The deposition rate is computed in a similar way, yielding

$$\begin{aligned}w^+(r) &= \int_0^1 dx\left[\rho_0^\star(x,r)\right]^3 + O\left(\frac{1}{L}\right) \\ &= (1-r)^3 + O\left(\frac{1}{L}\right).\end{aligned} \tag{35}$$

Here we used the fact that the inert vacancies have a flat steady-state profile, $\rho_0^\star(x,r) = 1 - r$.

Equation (33) corresponds to a one-dimensional random walk in r in the presence of a local potential which scales linearly with L. This implies that its steady-state solution obeys a large deviations principle of the form

$$P(r) = e^{L\mathcal{G}(r)}, \tag{36}$$

where $\mathcal{G}$ is the corresponding large deviations function. Inserting this form into Eq. (33) and expanding to first order in L yields

$$(e^{-3\mathcal{G}'(r)} - 1)w^+(r) + (e^{3\mathcal{G}'(r)} - 1)w^-(r) = 0. \tag{37}$$

This solution to the above equation is given by

$$\mathcal{G}(r) = -\frac{1}{3}\int_{r_0}^{r} dr' \ln[w^-(r')/w^+(r')], \tag{38}$$

where r_0 is chosen arbitrarily to be the minimal possible particle density, $r_0 = r - 3\min_\alpha(r_\alpha)$. The large deviations function, $\mathcal{G}(r)$, which is, in fact, proportional to the potential felt by the random walker, is plotted in Fig. 5 for a typical point in parameter space.

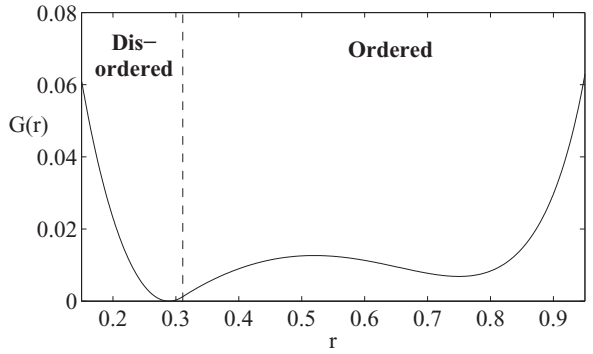

FIG. 5. The large deviations function of the overall density, r, for $\beta = 40$, $r_A = r_B = r/3 - 0.025$, and $\mu = -0.0515$. For this choice of parameters $\mathcal{G}(r)$ has two local minima, corresponding to a disordered and an ordered phase. The dashed line denotes the critical value of r, given in Eq. (21).

The large deviations function can be written in a more physically meaningful way as

$$\mathcal{G}(r) = \beta\mu r - \beta \int_{r_0}^{r} dr' \mu(r'), \tag{39}$$

where $\mu(r)$ is defined as

$$\mu(r) = \frac{1}{3\beta}\left\{ \ln\left[\int_0^1 dx \rho_A^\star(x,r)\rho_B^\star(x,r)\rho_C^\star(x,r)\right] - 3\ln(1-r)\right\}. \tag{40}$$

In [25], it is shown how the function $\mu(r)$ can be interpreted as the chemical potential of the conserving model, by measuring it using a generalization of Creutz's algorithm [44]. The measurement is done using a demon which takes triplets of ABC particles from the system and condenses them back onto 000 triplets. The two processes are performed randomly and slowly with rate p where $p \sim L^{-\gamma}$ and $\gamma > 2$. This algorithm results in a microscopic number of particles in the demon, which therefore does not alter the properties of the conserving system. The chemical potential is obtained from the distribution the number of particles in the demon, N_d, which is given by $P(N_d) \propto e^{-\mu(r)N_d}$, where r is the density of particles in the conserving system [45]. Unlike the equilibrium chemical potential, $\mu(r)$ is dynamics dependent. Its form depends on the fact that the demon is chosen to exchange only triplets of ABC particles with the system. In [25], it is demonstrated how $\mu(r)$ takes a different form when considering an alternative process that couples the demon to the system. This interpretation of $\mu(r)$ allows one to compare the phase diagrams of the conserving and nonconserving models on the same axes, as shown in Fig. 3.

The phase diagram of the conserving and nonconserving models can be studied by analyzing the behavior of $\mu(r)$ for various values of β and a_0. Since $\mu(r) = -\beta^{-1}\frac{d}{dr}\mathcal{G}(r) + \mu$ this analysis is equivalent to analyzing the properties of the large deviations of r, $\mathcal{G}(r)$. For high values $1/\beta$ (which for equal densities corresponds to the temperature), $\mu(r)$ is monotonous but displays a discontinuity in its first derivative, corresponding to a second order transition point, as shown in Fig. 6(a).

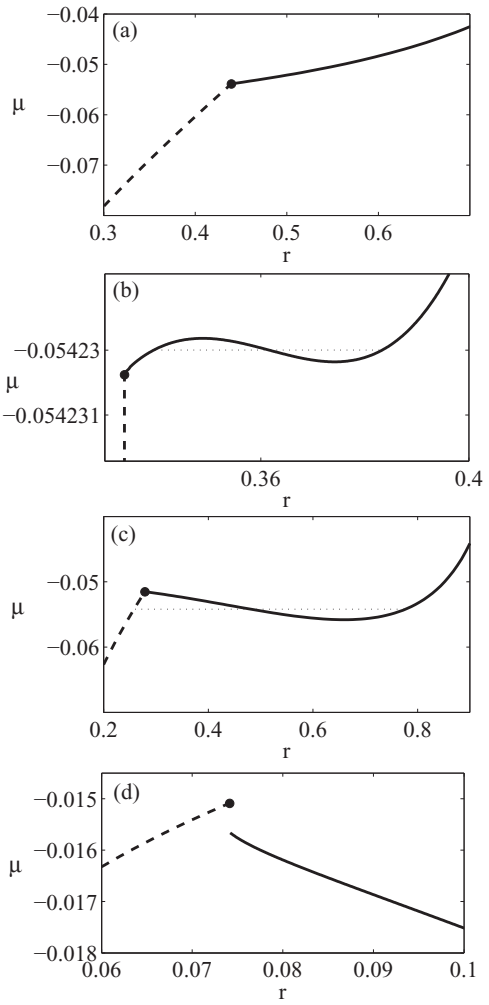

FIG. 6. Chemical potential calculated in the conserving model for the case of $r_A = r_B = r/3 - 0.01$. Panels (a),(b),(c),(d) correspond to $\beta = 25, 33.15, 40, 250$, respectively. The critical point is denoted by •. First order transition points, computed via Maxwell's construction, are denoted in (b) and (c) by dashed lines. The vertical scale in (b) is chosen to be extremely small in order to display to the variations in $\mu(r)$ around the first order transition point between the two ordered phases.

Below the nonconserving tricritical temperature, derived in the previous section, one finds a region of r where $\mu(r)$ can take three different values, as shown in Fig. 6(c). The intermediate density solution has negative compressibility and it is thus stable only in the conserving model. The nonconserving model exhibits a first order transition between the homogeneous (right most) and ordered (left most) solutions, which can be located using Maxwell's construction (dashed line). As discussed in the previous section, in the nonconserving model and in the case where $|a_0|$ is relatively small [presented in Fig. 3(b)], the second order transition line turns into a first order transition line at a critical end point (CEP). For temperatures slightly higher than the CEP, shown in the inset of Fig. 3(b), there is a second order transition between the disordered and the order phases as well as a first order transition between two ordered phases. The nature of this first order transition line can be understood from Fig. 6(b), which displays a first order

transition between a low density ordered phase and a high density ordered phase. The corresponding transition point can also be located using Maxwell's construction (dashed line). At very low temperatures, below the conserving tricritical point (24), $\mu(r)$ exhibits a jump at the critical point, as shown Fig. 3(d). This discontinuity is an indication of a first order transition, analyzed in [30], between a homogenous profile and an ordered profile with a finite amplitude. The values of μ on the two sides of the discontinuity define two stability limits that are denoted by the dashed lines in Fig. 3(a).

It is interesting to understand whether the inequivalence of the conserving and nonconserving phase diagrams can be regarded as ensemble inequivalence. To this end it is useful to write explicitly the approximation of nonconserving steady-state measure for $\gamma > 2$, given by

$$P_L(\boldsymbol{\zeta}) \approx \sum_N e^{L\mathcal{G}(N/L)} P_L(\boldsymbol{\zeta}; N), \tag{41}$$

where $P_L(\boldsymbol{\zeta}; N)$ is the conserving steady state. The above equation implies that the $P_L(\boldsymbol{\zeta})$ is a statistical ensemble of $P_L(\boldsymbol{\zeta}; N)$. Similar to $\mu(r)$, this statistical ensemble is not uniquely defined and depends on the choice of the nonconserving processes. This is in contrast to equilibrium systems, where $\mathcal{G}(r)$ is uniquely defined by the Hamiltonian and is given up to a constant by $\mathcal{G}(r) = -\beta F(r) + \beta\mu r$ with $F(r)$ denoting the Helmholtz free energy density. Based on this definition the difference between Figs. 3(a) and 3(b) can be regarded as a nonequilibrium ensemble inequivalence.

The above derivation of $\mathcal{G}(r)$ is rather general and can be applied to any stochastic model which exhibits a fast conserving dynamics and a slow nonconserving dynamics. One may consider several types of nonconserving dynamical steps of the same variable and/or steps of different sizes. In these cases one can still obtain a general solution for Eq. (33), independent of the details of w_- and w_+, that has a more complicated form than Eq. (38). Another possibility is to consider several nonconserving quantities. In this case the large deviations function of the slow variables is given by the steady-state solution of a higher-dimensional random walk which does not have a general form such as Eq. (38).

IV. *ABC* MODEL WITH NONEQUAL DENSITIES AND COMPARABLY SLOW NONCONSERVING DYNAMICS ($p \sim L^{-2}$)

In the previous section the nonconserving ABC model was analyzed in the limit $p \sim L^{-\gamma}$ and $\gamma > 2$, where the steady-state profile and the large deviations function of r can be computed analytically. In this section we study how these result are modified in the limit where

$$p = \phi L^{-2}, \tag{42}$$

and ϕ is a parameter that does not scale with L.

In Sec. IV A we demonstrate that the conserving and the nonconserving models exhibit for any finite ϕ different ordered profiles, as well as different critical lines. This additional inequivalence can be attributed to the sensitivity of nonequilibrium systems to the details of their dynamics rather than to the existence of long-range correlations. Remarkably, slightly below the critical line the nonconserving model exhibits a steady-state profile with a nonvanishing drift velocity.

In Sec. IV B we derive an expansion in small ϕ of the large deviations function of r using the macroscopic fluctuation theory. The leading order term in the expansion corresponds to the large deviations function, $\mathcal{G}(r)$, obtained for $\gamma > 2$ in Eq. (38). This confirms that $\gamma > 2$ is indeed the limit where the conserving and the nonconserving dynamics are well-separated. In the homogenous phase, the large deviations function in Eq. (38) is found to be valid for all values of ϕ. This conclusion is argued to be correct for a wide class of driven-diffusive models that exhibit a homogenous density profile.

A. Density profile, drift velocity, and critical line

For $p = \phi L^{-2}$ the dynamics of the density profile in the nonconserving ABC model (14) can be written as

$$\begin{aligned}\partial_\tau \rho_\alpha = {} & \beta \partial_x \left[\rho_\alpha \left(\rho_{\alpha+1} - \rho_{\alpha+2}\right)\right] + \partial_x^2 \rho_\alpha \\ & + \phi \left(\rho_0^3 - e^{-3\beta\mu} \rho_A \rho_B \rho_C\right).\end{aligned} \tag{43}$$

Although an analytic steady-state solution for the above equation is not available, it can easily be shown to be different from $\rho^\star(x,r)$, obtained in the conserving model ($\phi = 0$). As mentioned above, this inequivalence between the conserving and the nonconserving models is not necessarily due to the existence of long-range correlations in the system.

Equation (43) exhibits a homogenous solution around which it can be expanded. As demonstrated below, in this case one has to consider a moving density profile and thus use an expansion similar to Eq. (15) with x replaced with $x - vt$, yielding

$$\begin{aligned}\begin{pmatrix}\rho_A \\ \rho_B \\ \rho_C\end{pmatrix} = \sum_{m=-\infty}^{\infty} e^{2\pi i m(x-v\tau)} \Bigg[& \frac{a_m(\tau)}{\sqrt{3}} \begin{pmatrix}1 \\ e^{-2\pi i/3} \\ e^{2\pi i/3}\end{pmatrix} \\ & + \frac{a^\star_{-m}(\tau)}{\sqrt{3}} \begin{pmatrix}1 \\ e^{2\pi i/3} \\ e^{-2\pi i/3}\end{pmatrix} + \frac{b_m(\tau)}{3} \begin{pmatrix}1 \\ 1 \\ 1\end{pmatrix}\Bigg].\end{aligned} \tag{44}$$

Close to the critical line, we assume that $a_m, b_m \ll 1$ for all $m \neq 0$. It is important to note that the velocity, v, does not, in general, vanish on the critical line. By contrast, in the conserving model the existence of a moving density profile has been excluded for all values of β and a_0 in [32].

The main difference between the critical expansions for $\gamma < 2$ and for $\gamma = 2$ is that in the latter case the b_m amplitudes have a drift term in addition to the diffusive term. The drift term, which scales as ϕ, yields to leading order in a_m, b_m the following equation:

$$\begin{aligned}\partial_\tau b_m = {} & (2\pi i m v - 4\pi^2 m^2) b_m + 3\phi \Bigg\{ -3(1-b_0)^2 b_m \\ & - e^{-3\beta\mu} \Bigg[\frac{b_0^2 b_m}{9} - \frac{2b_0}{3}(a_0 a^\star_{-m} + a_m a^\star_0) \\ & + \frac{1}{\sqrt{3}}\left(a_0^2 a_m + a_0^{\star 2} a^\star_{-m}\right)\Bigg]\Bigg\} + O\left(a_m^2\right).\end{aligned} \tag{45}$$

Assuming a steady state, $\partial_\tau b_m = 0$, and considering β that are slightly below the critical line, where $b_m, a_m \ll 1$, one obtains a linear dependence between b_m and a_m, given by

$$b_m = \kappa_m a_m + \kappa_m^\star a_{-m}^\star + O\left(a_m^2\right), \tag{46}$$

where

$$\kappa_m \equiv \phi \frac{3e^{-3\beta\mu}\left(\sqrt{3}a_0^2 - 2ra_0^\star\right)}{12\pi^2 m^2 - 6\pi i m v + 27\phi(1-r)^2 + \phi r^2 e^{-3\beta\mu}}. \tag{47}$$

As expected, κ_m vanishes in the $\phi \to 0$ limit as well as for equal densities ($a_0 = 0$).

In order to complete the expansion one has to consider the evolution of a_m, obtained by the expansion of Eq. (43) in small a_m and b_m. The nonconserving term in Eq. (43) does not enter directly into the equation of a_m since it is proportional to the vector $(1,1,1)^T$, whereas a_m is the amplitude of the orthogonal vector $(1,e^{-2\pi i/3},e^{2\pi i/3})^T$. The leading order effect of the nonconserving dynamics comes from the term that couples b_m and a_0. Expanding Eq. (43) using the form in Eq. (44) and the expression for b_m in Eq. (46) yields to leading order

$$\begin{pmatrix} \partial_\tau a_m \\ \partial_\tau a_{-m}^\star \end{pmatrix} = -\frac{2\pi m}{3} A_m \begin{pmatrix} a_m \\ a_{-m}^\star \end{pmatrix} + O\left(a_m^2\right), \tag{48}$$

where A_m is given by

$$A_m = \begin{pmatrix} 6\pi m - \sqrt{3}\beta r - 3iv - \sqrt{3}\beta a_0 \kappa_m & 6\beta a_0^\star - \sqrt{3}\beta a_0^\star \kappa_m^\star \\ -6\beta a_0 + \sqrt{3}\beta a_0 \kappa_m & 6\pi m + \sqrt{3}\beta r - 3iv + \sqrt{3}\beta a_0^\star \kappa_m^\star \end{pmatrix}. \tag{49}$$

It is easy to see that for $k_m = 0$ and $v = 0$ the A_m matrices reduce to those in Eq. (19).

The critical point is defined by the lowest temperature $(1/\beta)$ for which $\det A_m = 0$ for one of the m's. The explicit form of this condition is given by

$$\begin{aligned} &9(2m\pi - iv)^2 - 6\sqrt{3}\beta(2im\pi + v)\mathrm{Im}[a_0\kappa_m] \\ &- 3\beta^2(r^2 - 12|a_0|^2 + 2r\mathrm{Re}[a_0\kappa_m] + 4\sqrt{3}|a_0|^2\mathrm{Re}[\kappa_m]) = 0, \end{aligned} \tag{50}$$

where Re and Im denote the real and imaginary parts, respectively. In general, $\mathrm{Im}[a_0\kappa_m] \neq 0$ and therefore the solution of Eq. (50) yields $v \neq 0$. The velocity, v, is given by the solution of a cubic equation and is thus omitted for the sake of brevity. This solution is studied below in the limit of $\phi \ll 1$ and plotted for a specific line in parameter space in Fig. 7. In the special case where $a_0 = |a_0|e^{\pi i \ell/3}$ for $\ell = 0,1,2$, one finds from Eq. (47) that $\mathrm{Im}[a_0\kappa_m] \propto v$, which in turn leads to a solution of Eq. (50) with $v = 0$. This condition can be shown to correspond to the case where at least two of the species have the same densities. This result conforms with the intuition that in the two-equal-densities case the system does not have a preferred drift direction and hence $v = 0$. The vanishing of the velocity is evident in Fig. 7 at $r_A = r_B$, $r_A = r_C$, or $r_B = r_C$.

In the two-equal-densities case the fact that $\mathrm{Im}[a_0\kappa_m] = 0$ simplifies Eq. (50). As in the previous sections the critical β is obtained when the $m = 1$ Fourier mode becomes unstable. The solution of Eq. (50) with $m = 1$ and $\mathrm{Im}[a_0\kappa_m] = 0$ yields

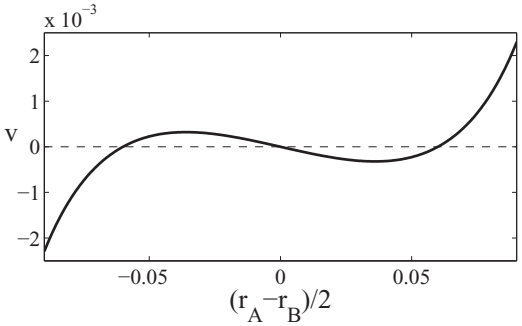

FIG. 7. Velocity of the unstable mode on the critical point for $r_A = 0.18 + x, r_B = 0.18 - x, r_C = 0.24$, and $\phi = 1$. The horizontal axis represents the value of x.

the following critical line in the two-equal-densities case:

$$\beta_c = \frac{2\pi\sqrt{3}}{\sqrt{r^2 - 12|a_0|^2 + 2ra_0\kappa_1 + 4\sqrt{3}|a_0|^2\mathrm{Re}[\kappa_1]}}. \tag{51}$$

As expected, in the $\phi \to 0$ limit, where $\kappa_1 \to 0$, this line coincides with the critical line in Eq. (21) obtained for $\gamma > 2$.

For arbitrary densities, the drift velocity can be studied analytically in the $\phi \ll 1$ limit. In this case, one would expect v to vanish with ϕ, and therefore Eq. (46) can be written as

$$\kappa_m = \phi \frac{\sqrt{3}a_0^2 - 2ra_0^\star}{4\pi^2 m^2} e^{-3\beta\mu} + o(\phi). \tag{52}$$

Similar to the $\gamma > 2$ case, the critical transition occurs for $\phi \ll 1$ when the $m = 1$ Fourier mode becomes unstable. Inserting Eq. (52) into Eq. (50) for $m = 1$ yields

$$v = -\frac{\phi}{\sqrt{3}}\mathrm{Im}[a_0\kappa_1]\beta_c + O(\phi^2), \tag{53}$$

where β_c denotes the critical β of the conserving model, given in Eq. (21). From Eqs. (52) and (53) one obtains that $v \propto \phi\mathrm{Im}[a_0^3]$, which implies that the drift velocity vanishes cubically with the deviation from the equal-density point, $|a_0|$. Equation (53) can also be expressed in terms of r_A, r_B, and r_C using the fact that $\mathrm{Im}[a_0^3] = -\frac{1}{2}(r_A - r_B)(r_B - r_C)(r_C - r_A)$ and $e^{-3\beta\mu} = (1-r)^3/r_A r_B r_C$, which yields

$$v = \phi\beta_c \frac{(1-r)^3(r_A - r_B)(r_B - r_C)(r_C - r_A)}{8\pi^2 r_A r_B r_C} + O(\phi^2). \tag{54}$$

The latter expression indeed vanishes in the two-equal-densities case.

B. Corrections to the large deviations function of r

In this section we study the large deviations properties of the nonconserving ABC model in the limit where $p = \phi L^{-2}$. In this limit the probability of a rare density profile can be expressed using the macroscopic fluctuation theory by extremizing the action of the model over all the possible instanton paths leading to the target profile [33–38]. Here we specifically consider events where a rare number of particles is observed. We show that in the $\phi \to 0$ limit these events are realized by an instanton that passes only through steady-state

profiles of the conserving system, i.e., $\boldsymbol{\rho}(x,\tau) = \boldsymbol{\rho}^{\star}(x,r(\tau))$, where $r(\tau)$ can be computed analytically. The large deviations function of r, obtained using this instanton path, coincides in the $\phi \to 0$ limit with the one computed for $p \sim L^{-\gamma}$ with $\gamma > 2$ in Sec. III B. In the homogenous phase we find that this instanton path and the corresponding large deviations function remain valid for all ϕ. In the ordered phase we write an expansion of the instanton in small ϕ and derive equations that describe its first order correction. This expansion is presented in a relatively general form, which can be easily adapted to other driven-diffusive models.

The macroscopic fluctuation theory deals with the probability to observe a trajectory of the macroscopic current of particles within a given time interval, denoted here by $[0,T]$. In our case we consider three conserving currents, $\mathbf{j}(x,\tau) \equiv [j_A(x,\tau), j_B(x,\tau), j_C(x,\tau)]^T$, which result from local exchanges of particles, and a nonconserving current, $k(x,\tau)$, which results from evaporation and deposition of triplets of particles. The density profile is obtained from those two currents via the continuity equation

$$\partial_\tau \boldsymbol{\rho}(x,\tau) = -\partial_x \mathbf{j}(x,\tau) + \phi \mathbf{u} k(x,\tau), \tag{55}$$

where $\mathbf{u} = (1,1,1)^T$. It is important to note that $k(x,\tau)$ is the nonconserving current of triplets of particles and not of single particles.

The probability of a trajectory in current space, defined by $\mathbf{j}(x,\tau)$ and $k(x,\tau)$, is given by a large deviations principle,

$$\begin{aligned}&\Pr[\mathbf{j}(x,\tau),k(x,\tau)|\boldsymbol{\rho}(x,0)] \\ &\quad \sim e^{-L\int_0^T d\tau \int_0^1 dx [\mathcal{L}_c(\boldsymbol{\rho}(x,\tau),\mathbf{j}(x,\tau)) + \phi \mathcal{L}_{nc}(\boldsymbol{\rho}(x,\tau),k(x,\tau))]},\end{aligned} \tag{56}$$

where $\mathcal{L}_c$ and $\mathcal{L}_{nc}$ denote the conserving and the nonconserving Lagrangian densities, respectively. These functionals, whose explicit form is given below, correspond to the "probability cost" of the conserving and of the nonconserving noises, respectively. The steady-state probability of a density profile $\bar{\boldsymbol{\rho}}(x)$ can be obtained from Eq. (56) by integrating it over all the trajectories for which $\boldsymbol{\rho}(x,T) = \bar{\boldsymbol{\rho}}(x)$ in the limit of $T \to \infty$, yielding

$$\begin{aligned}&\Pr[\boldsymbol{\rho}(x) = \bar{\boldsymbol{\rho}}(x)] \\ &= \lim_{T\to\infty} \int D\boldsymbol{\rho}\Big|_{\boldsymbol{\rho}(x,T)=\bar{\boldsymbol{\rho}}(x)} D\mathbf{j} Dk \Pr[\mathbf{j}(x,\tau),k(x,\tau)|\boldsymbol{\rho}(x,0)] \\ &\quad \times \prod_\alpha \delta[\partial_\tau \rho_\alpha(x,\tau) + \partial_x j_\alpha(x,\tau) - \phi k(x,\tau)],\end{aligned} \tag{57}$$

where $\boldsymbol{\rho}(x,0)$ can be chosen arbitrarily.

The conserving Lagrangian density, $\mathcal{L}_c$, has been derived for the standard ABC model ($p = 0, r = 1$) in [43]. It is important to note that this expression cannot be mapped onto the $r < 1$ case, as done in Eq. (30) for the steady-state density profile. This is because for $r < 1$ one has to consider fluctuations in $\rho_A(x) + \rho_B(x) + \rho_C(x)$ which were not allowed for $r = 1$. We now sketch the derivation of $\mathcal{L}_c$ for $r < 1$ by following the lines of derivation presented in [43]. First we consider the Langevin equation for the macroscopic current, $\mathbf{j}(x,t)$, given by

$$j_\alpha(x,\tau) = -\chi_\alpha(\boldsymbol{\rho}(x,\tau)) - \partial_x \rho(x,\tau) + \frac{1}{\sqrt{L}}\eta_\alpha, \tag{58}$$

where $\chi_\alpha(\boldsymbol{\rho}) = \beta\rho_\alpha(x,t)[\rho_{\alpha+1}(x,t) + \rho_{\alpha+2}(x,t)]$ denotes the drift term. The variables η_α denote Gaussian white noise, whose correlations are given by

$$\langle \eta_\alpha(x,\tau)\eta_{\alpha'}(x',\tau')\rangle = \delta(x-x')\delta(\tau-\tau')\Sigma_{\alpha,\alpha'}(\boldsymbol{\rho}(x,\tau)), \tag{59}$$

where $\Sigma_{\alpha,\alpha'}(\boldsymbol{\rho})$ is the conductivity matrix. The latter can be obtained by calculating the local covariance of the conserving currents for $\beta = 0$ (see discussion in Appendix B of [32] and in Sec. 2.3 of [43]), yielding

$$\Sigma_{\alpha\alpha'}(\boldsymbol{\rho}) = \begin{cases} 2\rho_\alpha(1-\rho_\alpha) & \alpha = \alpha', \\ -2\rho_\alpha\rho_{\alpha'} & \alpha \neq \alpha'. \end{cases} \tag{60}$$

The probability of a current trajectory $\mathbf{j}(x,\tau)$ is obtained by integrating over the probability distribution of the noise variable and performing the Martin-Siggia-Rose procedure. This yields a large deviations function given by the integral over the following Lagrangian density:

$$\mathcal{L}_c(\boldsymbol{\rho},\mathbf{j}) = [\mathbf{j} + \partial_x \boldsymbol{\rho} + \boldsymbol{\chi}(\boldsymbol{\rho})]^T\, \Sigma^{-1}(\boldsymbol{\rho})\, [\mathbf{j} + \partial_x \boldsymbol{\rho} + \boldsymbol{\chi}(\boldsymbol{\rho})]\,. \tag{61}$$

The nonconserving Lagrangian density, $\mathcal{L}_{nc}$, was derived for a general driven-diffusive system in [46–48]. We now repeat the heuristic derivation of $\mathcal{L}_{nc}$, presented for a general driven-diffusive model in [47], in the context of the nonconserving ABC model. The local nonconserving current is given by the combination of two Poisson processes: condensation of triplets of particles with rate $\phi\mathcal{C}(\boldsymbol{\rho}(x,\tau))$ and annihilation of triplets of particles, with rate $\phi\mathcal{A}(\boldsymbol{\rho}(x,\tau))$, where

$$\mathcal{A}(\boldsymbol{\rho}) = e^{-3\beta\mu}\rho_A\rho_B\rho_C, \quad \mathcal{C}(\boldsymbol{\rho}) = (1-\rho_A-\rho_B-\rho_C)^3. \tag{62}$$

For a small segment of the system, dx, and a small time interval, $d\tau$, the probability to observe $k\phi dx d\tau$ triplets of particles added or removed (depending on the sign of k) due to the nonconserving processes is given by

$$\begin{aligned}&\Pr\left[\int_x^{x+dx}\int_\tau^{\tau+\phi d\tau} dx d\tau k(x,\tau) = k\phi dx d\tau\right] \\ &= \sum_{n=\max(0,Lk\phi d\tau dx)}^{\infty} P^{(\text{Pois.})}_{\phi\mathcal{C}(\boldsymbol{\rho})dxdt}(n) P^{(\text{Pois.})}_{\phi\mathcal{A}(\boldsymbol{\rho})dxdt}(n - Lk\phi dxdt) \\ &\sim e^{-\phi\mathcal{L}_{nc}(\boldsymbol{\rho},k)d\tau dx},\end{aligned} \tag{63}$$

where $P^{(\text{Pois.})}_\lambda$ denotes the Poisson distribution function with a mean of λ. The nonconserving action is obtained by performing the saddle point approximation over the above sum, yielding

$$\begin{aligned}\mathcal{L}_{nc}(\boldsymbol{\rho},k) &= \mathcal{C}(\boldsymbol{\rho}) + \mathcal{A}(\boldsymbol{\rho}) - \sqrt{k^2 + 4\mathcal{A}(\boldsymbol{\rho})\mathcal{C}(\boldsymbol{\rho})} \\ &\quad + k\ln\left[\frac{\sqrt{k^2 + 4\mathcal{A}(\boldsymbol{\rho})\mathcal{C}(\boldsymbol{\rho})} + k}{2\mathcal{C}(\boldsymbol{\rho})}\right].\end{aligned} \tag{64}$$

This functional form is identical to the one obtained in [47] for a general $\mathcal{A}$ and $\mathcal{C}$. Since the conserving and the nonconserving processes occur independently, the corresponding Lagrangian densities can be added together, yielding Eq. (56).

The integral in Eq. (57) can be evaluated using the saddle point approximation, whereby the probability of a density profile is governed by the action over the most probable path

to reach $\bar{\boldsymbol{\rho}}(x)$ at time $T \to \infty$. In order to find this path it is useful to consider two functions, $\mathbf{H}(x,\tau)$ and $G(x,\tau)$, defined as

$$\Sigma(\boldsymbol{\rho})\partial_x \mathbf{H} = \mathbf{j} + \partial_x \boldsymbol{\rho} + \boldsymbol{\chi}(\boldsymbol{\rho}), \tag{65}$$

$$k = \mathcal{C}(\boldsymbol{\rho})e^{G} - \mathcal{A}(\boldsymbol{\rho})e^{-G}. \tag{66}$$

Physically, $\mathbf{H}(x,\tau)$ and $G(x,\tau)$ correspond to the fields exerted by the external baths that drive the conserving and the nonconserving currents, respectively.

In terms of $\mathbf{H}(x,\tau)$ and $G(x,\tau)$, the Lagrangian densities can be written as

$$\mathcal{L}_c(\boldsymbol{\rho},H) = \tfrac{1}{2}(\partial_x \mathbf{H})^T \Sigma(\boldsymbol{\rho})\, \partial_x \mathbf{H}, \tag{67}$$

$$\begin{aligned}\mathcal{L}_{nc}(\boldsymbol{\rho},G) = {} & \mathcal{C}(\boldsymbol{\rho})(1 - e^{G} + Ge^{G}) \\ & + \mathcal{A}(\boldsymbol{\rho})(1 - e^{-G} - Ge^{-G}).\end{aligned} \tag{68}$$

By expanding the action,

$$\mathcal{I}(\boldsymbol{\rho},\mathbf{H},G) \equiv \int_0^T d\tau \int_0^1 dx[\mathcal{L}_c(\boldsymbol{\rho},\mathbf{H}) + \mathcal{L}_{nc}(\boldsymbol{\rho},G)], \tag{69}$$

in small variations in $\mathbf{H}(x,\tau)$ and $G(x,\tau)$ around the extremizing trajectory of $\mathcal{I}$, it is shown in Appendix B that this trajectory obeys the following equations:

$$G = H_A + H_B + H_C, \tag{70}$$

$$\begin{aligned}\partial_\tau H_\alpha = {} & -\partial_x^2 H_\alpha + \partial_x \mathbf{H}^T \partial_{\rho_\alpha} \boldsymbol{\chi}(\boldsymbol{\rho}) - \tfrac{1}{2}(\partial_x \mathbf{H})^T \partial_{\rho_\alpha} \Sigma(\boldsymbol{\rho})\, \partial_x \mathbf{H} \\ & + \phi[\partial_{\rho_\alpha} \mathcal{C}(\boldsymbol{\rho})(1 - e^{G}) + \partial_{\rho_\alpha} \mathcal{A}(\boldsymbol{\rho})(1 - e^{-G})],\end{aligned} \tag{71}$$

where $\boldsymbol{\rho}$ can be written in terms of $\mathbf{H}$ and G using the continuity equation (55), which yields

$$\begin{aligned}\partial_\tau \rho_\alpha = {} & \partial_x^2 \rho_\alpha + \partial_x \chi_\alpha(\boldsymbol{\rho}) - \partial_x[\Sigma(\boldsymbol{\rho})\partial_x \mathbf{H}]_\alpha \\ & + \phi[\mathcal{C}(\boldsymbol{\rho})e^{G} - \mathcal{A}(\boldsymbol{\rho})e^{-G}].\end{aligned} \tag{72}$$

It is useful to note that the derivation of Eqs. (65)–(72) can be regarded as a transformation into a Hamiltonian picture. In this respect, the fields $\mathbf{H}(x,\tau)$ and $G(x,\tau)$ are the momenta conjugate to $-\int_0^\tau d\tau' \partial_x \mathbf{j}(x,\tau')$ and $\int_0^\tau d\tau' k(x,\tau')$, respectively, and Eqs. (70)–(72) play the role of Hamilton's equations

Another important point is the form of optimal trajectory obtained if one minimizes $\mathcal{I}$ over $\boldsymbol{\rho}(x,T)$ as well. In this case, $\mathbf{H}$ are allowed to fluctuate freely. The quadratic form of $\mathcal{L}_c$ in $\mathbf{H}$ implies that the optimal trajectory is obtained in this case by considering $\mathbf{H}(x,\tau) = 0$. Inserting this solution into Eqs. (70) and (72) yields the deterministic dynamics of the profile in Eq. (14).

As discussed above, the solution to Eqs. (70)–(72) in the $\phi \ll 1$ limit is expected to yield a density profile of the form $\boldsymbol{\rho}(x,t) = \boldsymbol{\rho}^\star(x,r(\tau)) + O(\phi)$. Inserting this ansatz into Eq. (72) yields $\mathbf{H}(x,\tau)$ which is constant in space up to deviations proportional to ϕ. In addition, it is evident that $r(\tau)$ evolves on a slow time scale defined by $\phi\tau$. One can therefore consider the following expansion of the instanton path:

$$H_\alpha(x,\tau) = \frac{1}{3} g(\phi\tau) + \sum_{k=1}^{\infty} \phi^k \delta_{H,\alpha}^{(k)}(x,\phi\tau), \tag{73}$$

$$\rho_\alpha(x,\tau) = \rho_\alpha^\star(x,r(\phi\tau)) + \sum_{k=1}^{\infty} \phi^k \delta_{\rho,\alpha}^{(k)}(x,\phi\tau). \tag{74}$$

The functions appearing in the above expansion can be computed by inserting Eqs. (73)–(74) into Eqs. (70)–(72) and solving them order by order in ϕ. The leading order terms, $g(s)$ and $r(s)$ (with s denoting $\phi\tau$), are obtained from integrating over x and summing over α the $O(\phi)$ terms in Eqs. (70)–(72). This integral and sum of Eq. (72) yields

$$\frac{dr}{ds} = 3\int_0^1 dx[\mathcal{C}(\boldsymbol{\rho}_s^\star)e^{g(s)} - \mathcal{A}(\boldsymbol{\rho}_s^\star)e^{-g(s)}], \tag{75}$$

where $\boldsymbol{\rho}_s^\star \equiv \boldsymbol{\rho}^\star(x,r(s))$. Similarly, multiplying Eq. (71) by $\partial_r \rho_\alpha^\star(x,r(s))$ and integrating over x yields

$$\begin{aligned}\frac{dg}{ds} = {} & \int_0^1 dx \sum_\alpha \partial_r \rho_\alpha^\star(x,r(s))[\partial_{\rho_\alpha} \mathcal{C}(\boldsymbol{\rho}_s^\star)(1 - e^{g(s)}) \\ & + \partial_{\rho_\alpha} \mathcal{A}(\boldsymbol{\rho}_s^\star)(1 - e^{-g(s)})].\end{aligned} \tag{76}$$

Here all the terms that contain $\delta_{H,\alpha}^{(1)}$ were removed using integration by parts and the fact that $\partial_x^2 \rho_\alpha^\star + \partial_x \chi_\alpha(\boldsymbol{\rho}^\star) = 0$. Equation (76) has a solution of the form,

$$g(s) = \ln\left[\int_0^1 dx \mathcal{A}(\boldsymbol{\rho}_s^\star)\right] - \ln\left[\int_0^1 dx \mathcal{C}(\boldsymbol{\rho}_s^\star)\right], \tag{77}$$

which when inserted into Eq. (75) yields

$$\frac{dr}{ds} = 3\int_0^1 dx[\mathcal{A}(\boldsymbol{\rho}_s^\star) - \mathcal{C}(\boldsymbol{\rho}_s^\star)]. \tag{78}$$

In general, since $\boldsymbol{\rho}^\star(x,r)$ has a rather complicated form, the solution of Eq. (78) can only be obtained numerically. Nevertheless, in the following paragraphs we draw some interesting conclusions from the general form of Eq. (78).

To leading order in ϕ, Eq. (78) describes the time reversal of the relaxation trajectory of r from an atypical initial value. The relaxation trajectory can be obtained by inserting a solution of the form of Eq. (74) into Eq. (72) with $\mathbf{H}(x,\tau) = 0$ and keeping the leading order in ϕ. This time-reversal symmetry conforms with our intuition that in the limit of very slow nonconserving dynamics, the dynamics of r can be described as an equilibrium one-dimensional random walk. Since for $\gamma > 2$ we know that this instanton path is the most probable one that realizes a rare value of r, it is plausible to assume the expansion around it for $\gamma = 2$ and $\phi \ll 1$ is also the global minimum of $\mathcal{I}$.

Under this assumption, the probability to observe a rare value of the overall density is obtained by evaluating the action (69) over the instanton path in Eqs. (73)–(74). This statement can be written formally as

$$\begin{aligned}P(\bar{r}) = {} & P[\boldsymbol{\rho}(x) = \boldsymbol{\rho}^\star(x,\bar{r}) + O(\phi)] \\ \sim {} & \lim_{\phi T \to \infty} e^{-L\int_0^{\phi T} ds \int_0^1 dx[\mathcal{L}_c(\boldsymbol{\rho}_s^\star, \frac{1}{3}g(s)) + \mathcal{L}_{nc}(\boldsymbol{\rho}_s^\star, g(s))] + O(\phi)},\end{aligned} \tag{79}$$

where $g(0)$ is chosen such that $r(\phi T) = \bar{r}$. Using Eqs. (77)–(78) the above exponential can be written as

$$P(\bar{r}) \sim e^{\frac{L}{3}\int^{\bar{r}} dr' \{\ln[\int_0^1 dx \mathcal{C}(\boldsymbol{\rho}^\star(x,r'))] - \ln[\int_0^1 dx \mathcal{A}(\boldsymbol{\rho}^\star(x,r'))]\} + O(\phi)}. \tag{80}$$

As expected, the leading order term of this large deviations function is identical to $\mathcal{G}(r)$ obtained for $\gamma > 2$ in Sec. III B.

Corrections to $\mathcal{G}(r)$ can be obtained by calculating the $O(\phi)$ corrections to the instanton path. Considering the $O(\phi)$ terms when expanding Eqs. (71)–(72), we find that

$$\begin{aligned} 0 = {} & \partial_x^2 \delta^{(1)}_{\rho,\alpha} + \partial_x \left[\delta^{(1)}_{\rho,\alpha} \partial_{\rho_\alpha} \chi_\alpha(\boldsymbol{\rho}^\star_s)\right] - \partial_x \left[\Sigma(\boldsymbol{\rho}^\star)\partial_x \boldsymbol{\delta}^{(1)}_H\right]_\alpha \\ & + \mathcal{C}(\boldsymbol{\rho}^\star_s) e^{g(s)} - \mathcal{A}(\boldsymbol{\rho}^\star_s) e^{-g(s)} \\ & - \partial_r \boldsymbol{\rho}^\star_s \int_0^1 dx [\mathcal{C}(\boldsymbol{\rho}^\star_s) e^{g(s)} - \mathcal{A}(\boldsymbol{\rho}^\star_s) e^{-g(s)}], \end{aligned} \tag{81}$$

$$\begin{aligned} 0 = {} & -\partial_x^2 \delta^{(1)}_{H,\alpha} + \partial_x \boldsymbol{\delta}^{(1),T}_H \partial_{\rho_\alpha} \boldsymbol{\chi}(\boldsymbol{\rho}^\star_s) + \partial_{\rho_\alpha} \mathcal{C}(\boldsymbol{\rho}^\star_s)(1 - e^{g(s)}) \\ & + \partial_{\rho_\alpha} \mathcal{A}(\boldsymbol{\rho}^\star_s)(1 - e^{-g(s)}) - \int_0^1 dx \partial_r \boldsymbol{\rho}^\star_s [\partial_{\rho_\alpha} \mathcal{C}(\boldsymbol{\rho}^\star_s)(1 - e^{g(s)}) \\ & + \partial_{\rho_\alpha} \mathcal{A}(\boldsymbol{\rho}^\star_s)(1 - e^{-g(s)})], \end{aligned} \tag{82}$$

where as before $s \equiv \phi\tau$. Since $r(s)$ does not have a simple analytic expression in the ABC model, the above equations can only be solved numerically.

In the homogenous phase, where $\rho^\star_\alpha(x,r) = r_\alpha$, the source terms in Eqs. (81)–(82) vanish, yielding a set of homogenous partial differential equations that exhibit a trivial solution, $\delta^{(1)}_{H,\alpha} = \delta^{(1)}_{\rho,\alpha} = 0$. In fact, in this case the leading order term of the instanton, $H_\alpha(x,\tau) = \frac{1}{3} g(\phi\tau)$ and $\boldsymbol{\rho}(x,\tau) = \boldsymbol{\rho}^\star(x, r(\phi\tau))$, can be shown to satisfy Eqs. (70)–(72) to all orders in ϕ. This conclusion does not depend on the specific form of $\Sigma(\boldsymbol{\rho})$ and $\boldsymbol{\chi}(\boldsymbol{\rho})$, and can be shown to remain valid also when considering a density-dependent diffusion coefficient. This implies that for any homogenous driven-diffusive system with a slow particle-nonconserving dynamics ($p \sim L^{-\gamma}$ with $\gamma \geqslant 2$) that is characterized by space-independent functions $\mathcal{A}(r)$ and $\mathcal{C}(r)$, the large deviations principle of the overall particle-density is given by

$$P(\bar{r}) \sim e^{\frac{L}{\omega}\int^{\bar{r}} dr' [\ln \mathcal{C}(r') - \ln \mathcal{A}(r')]}. \tag{83}$$

Here ω are the number of particles added and removed in each condensation and annihilation process. In the nonconserving ABC model $\omega = 3$.

Another interesting result of the above expansion concerns the time-reversal symmetry found in the dynamics of r, whereby its excitation trajectory to a rare density, $\bar{r}$, is equal to the time-reversal of the relaxation path which starts from $r = \bar{r}$. This symmetry is broken for the local nonconserving current of particles, $k(x,\tau)$, for systems where $\mathcal{C}(\boldsymbol{\rho}^\star)$ and $\mathcal{A}(\boldsymbol{\rho}^\star)$ are not homogenous in space. On the one hand, in such cases the relaxation path of k, obtained by setting $G = 0$ in Eq. (66), is given by

$$k_\downarrow(x,\tau) = \mathcal{C}(\boldsymbol{\rho}^\star_{\phi\tau}) - \mathcal{A}(\boldsymbol{\rho}^\star_{\phi\tau}). \tag{84}$$

On the other hand, the excitation path, obtained by inserting $r(s)$ and $g(s)$ into Eq. (66), is given by

$$k_\uparrow(x,\tau) = \mathcal{C}(\boldsymbol{\rho}^\star_{\phi\tau}) \frac{\int_0^1 dx' \mathcal{A}(\boldsymbol{\rho}^\star_{\phi\tau})}{\int_0^1 dx' \mathcal{C}(\boldsymbol{\rho}^\star_{\phi\tau})} - \mathcal{A}(\boldsymbol{\rho}^\star_{\phi\tau}) \frac{\int_0^1 dx' \mathcal{C}(\boldsymbol{\rho}^\star_{\phi\tau})}{\int_0^1 dx' \mathcal{A}(\boldsymbol{\rho}^\star_{\phi\tau})}, \tag{85}$$

and therefore, in general, $k_\uparrow(x,\tau) \neq -k_\downarrow(x,-\tau)$. Of course, the integral over the local current does obey time-reversal symmetry, $\int_0^1 dx k_\uparrow(x,\tau) = -\int_0^1 dx k_\downarrow(x,-\tau)$, leading to the symmetry observed in the dynamics of r. The breaking of the time-reversal symmetry of $k(x,\tau)$ occurs in the ordered phase of the ABC model, where $\rho^\star$ is not homogenous [49]. Hence, the nonequilibrium nature of the system is maintained even in the $\phi \to 0$ limit.

V. CONCLUSIONS

The phase diagram of the ABC model with slow nonconserving processes is analyzed in the case where the overall densities of the three species are not equal and the model is thus out of equilibrium. The phase diagram exhibits features similar to those characterizing equilibrium systems with long-range interactions such as ensemble inequivalence and negative compressibility. It also exhibits features which are specific to nonequilibrium systems, such as steady states with moving density profiles.

In the first part of the paper we focused on the case where the nonconserving processes occur at a vanishingly slow rate, $p \sim L^{-\gamma}, \gamma > 2$, compared with rates of the conserving dynamics, $\tau^{-1} \sim L^{-2}$. In this limit, the dynamics of the overall density, r, is shown to obey detailed balance, although the model itself does not. This allows one to derive the large deviations function of r and draw from it the phase diagram of the nonconserving model using equilibrium concepts such as the definition of a chemical in the conserving model and the calculation of the first order transition points using the Maxwell construction. As is typical in equilibrium systems with long-range interactions the conserving and nonconserving models are found to exhibit the same critical lines but different first order lines.

In the second part of the paper we studied the limit where the conserving and nonconserving processes occur at comparable time scales, defined as $p = \phi L^2$. In this case the models are found to differ not only in their first order lines but also in their second order ones. In addition, it is found that in the ordered phase the nonconserving model exhibits a moving density profile with nonvanishing velocity in the thermodynamic limit.

Using macroscopic fluctuation theory, we derived an expansion in small ϕ of the instanton path leading to a rare value of r. The leading order term of the action over this instanton is identical to the expression of $\mathcal{G}(r)$ obtained for $\gamma > 2$. This implies that $\gamma > 2$ is indeed the limit where the conserving and nonconserving time scale are well separated. An interesting result of this expansion is that all the correction terms in ϕ vanish in the homogenous phase, implying that the expression of $\mathcal{G}(r)$ obtained for $\gamma > 2$ is correct in the homogenous phase for $\gamma = 2$ as well. This conclusion is valid for a large class of driven-diffusive models that exhibit a homogenous steady-state profile.

ACKNOWLEDGMENTS

We thank A. Bar, L. Bertini, M. R. Evans, O. Hirschberg, and J. L. Lebowitz for helpful discussions. The support of the Israel Science Foundation (ISF) and of the Minerva Foundation with funding from the Federal German Ministry for Education and Research is is gratefully acknowledged. The authors are grateful for the kind hospitality of the Korean Institute of Advanced Studies (KIAS), where part of this work was conducted.

APPENDIX A: CRITICAL EXPANSION OF THE *ABC* MODEL WITH NONEQUAL DENSITIES AND VANISHINGLY SLOW NONCONSERVING DYNAMICS ($p \ll L^{-2}$)

In this appendix we carry out the critical expansion of the conserving and the nonconserving ABC models, in the limit $p \sim L^{-\gamma}$ with $\gamma > 2$, up to the forth order. The expansion for the sixth order terms in both cases have been derived but will not be displayed due to their length. They are used to determine the nature of the multicritical point which connects the second and first order transition manifolds.

The starting point of the expansion is the dynamics of the density profile, given in the conserving model by

$$\partial_\tau \rho_\alpha = \beta \partial_x \left[\rho_\alpha \left(\rho_{\alpha+1} - \rho_{\alpha+2}\right)\right] + \partial_x^2 \rho_\alpha. \tag{A1}$$

The nonconserving equation is obtained by adding a term of the form $L^2 p(\rho_0^3 - e^{-3\beta\mu}\rho_A\rho_B\rho_C)$ to the right hand side of Eq. (A1). As discussed in Sec. III A, in both the conserving and the nonconserving models the density profile can be expanded near the critical line in terms of the following Fourier modes:

$$\begin{pmatrix}\rho_A\\ \rho_B\\ \rho_C\end{pmatrix} = \sum_{m=-\infty}^{\infty} e^{2\pi i m x}\left[\frac{a_m(\tau)}{\sqrt{3}}\begin{pmatrix}1\\ e^{-2\pi i/3}\\ e^{2\pi i/3}\end{pmatrix} + \frac{a^\star_{-m}(\tau)}{\sqrt{3}}\begin{pmatrix}1\\ e^{2\pi i/3}\\ e^{-2\pi i/3}\end{pmatrix} + \frac{b_m(\tau)}{3}\begin{pmatrix}1\\ 1\\ 1\end{pmatrix}\right]. \tag{A2}$$

We first analyze the expansion of the conserving ABC model. Inserting Eq. (A2) into Eq. (A1) yields a set of decoupled equations of motion, given by

$$\partial_\tau a_m = -\frac{2\pi m}{3}\left[(6\pi m - \sqrt{3}\beta r)a_m + 3\beta\sum_{m'=-\infty}^{\infty} a^\star_{-m-m'}a^\star_{m'}\right], \tag{A3}$$

$$\partial_\tau b_m = -4\pi^2 m^2 b_m. \tag{A4}$$

The latter equation implies that in the steady state $b_m = 0$ for $m \neq 0$ and $b_0 = r$. This corresponds to a flat profile of the vacancies which is a result of their unbiased dynamics. It is useful to rewrite Eq. (A3) in the following vector form:

$$\begin{pmatrix}\partial_\tau a_m\\ \partial_\tau a^\star_{-m}\end{pmatrix} = -\frac{2\pi m}{3}\left[A_m\begin{pmatrix}a_m\\ a^\star_{-m}\end{pmatrix} + 3\beta\sum_{m'=-\infty}^{\infty}\begin{pmatrix}a^\star_{-m-m'}a^\star_{m'}\\ -a_{m-m'}a_{m'}\end{pmatrix}\right], \tag{A5}$$

where

$$A_m = \begin{pmatrix}6\pi m - \sqrt{3}\beta r & 6\beta a_0^\star\\ -6\beta a_0 & 6\pi m + \sqrt{3}\beta r\end{pmatrix}. \tag{A6}$$

The eigenvalues of $-\frac{2\pi m}{3}A_m$ are

$$\epsilon_\pm^{(m)}(\beta,r,a_0) = \frac{2\pi m}{3}[-6m\pi \pm \beta\sqrt{3(r^2 - 12|a_0|^2)}], \tag{A7}$$

and the corresponding left and right eigenvectors are independent of m and given by

$$v_\pm^R = \frac{1}{C_\pm}\begin{pmatrix}r \pm \sqrt{r^2 - 12|a_0|^2}\\ 2\sqrt{3}a_0\end{pmatrix}, \tag{A8}$$

$$v_\pm^L = \frac{1}{C_\pm}\begin{pmatrix}-r \mp \sqrt{r^2 - 12|a_0|^2}\\ 2\sqrt{3}a_0^\star\end{pmatrix}, \tag{A9}$$

where $C_\pm = 2\sqrt{r^2 - 12|a_0|^2}(r \mp \sqrt{r^2 - 12|a_0|^2})$ is a normalization factor. When the highest eigenvalue vanishes, $\epsilon_+^{(1)} = 0$, the corresponding Fourier mode becomes unstable, leading to an ordered profile. The critical line is defined as $\epsilon_+^{(1)}(\beta_c,r,a_0) = 0$, where β_c is given in Eq. (21).

In order to determine whether the conserving model exhibits a second order phase transition on the critical line one has to check whether for $\beta = \beta_c(1+\delta)$ the model exhibits an order phase whose amplitude vanishes with δ. To this end, it is useful to denote the first unstable Fourier mode as

$$\begin{pmatrix}a_1\\ a^\star_{-1}\end{pmatrix} = \varphi v_+^R + O(\varphi^2)v_+^L, \tag{A10}$$

where φ is given by up to a constant by some positive power of δ, which will be determined below. Assuming a steady state, $\partial_t a_m = 0$, and inserting Eq. (A10) into Eq. (A5) for $m = 2$ yields to leading order

$$\begin{pmatrix}a_2\\ a^\star_{-2}\end{pmatrix} = 3\beta_c\varphi^2 A_2^{-1}\begin{pmatrix}-(v^R_{+,2})^2\\ (v^R_{+,1})^2\end{pmatrix} + O(\varphi^4), \tag{A11}$$

where $v^R_{+,1}$ and $v^R_{+,2}$ denote the two elements of v^R_+. Inserting this back into Eq. (A5) for $m = 1$, yields the fourth order term in its expansion in powers of φ, given by

$$0 = 4\pi^2\delta\varphi + G_4^c(r,a_0)\varphi|\varphi|^2 + O(\varphi|\varphi|^4), \tag{A12}$$

where the $4\pi^2$ factor is due to fact that $\epsilon_+^{(1)}(\beta_c(1+\delta),r,a_0) = 4\pi^2\delta$ and

$$\begin{aligned} G_4^c(r,a_0) &= \frac{1}{\varphi|\varphi|^2}6\beta_c v_+^L\begin{pmatrix}a^\star_{-2}a^\star_1\\ -a_2a_{-1}\end{pmatrix}\\ &= \frac{32\pi^2(r^2 + r\sqrt{r^2 - 12|a_0|^2} - 6|a_0|^2)}{(r^2 - 12|a_0|^2)^2(r + \sqrt{r^2 - 12|a_0|^2})}\\ &\quad\times[r^3 - 18r|a_0|^2 - 12\sqrt{3}|a_0|^3\cos(3\theta)], \end{aligned} \tag{A13}$$

with $\theta \equiv \arg(a_0)$.

For $G_4^c(r,a_0) > 0$ one finds that $\varphi \sim \delta^{1/2}$, which implies that the model exhibits a second order phase transition on the critical line. On the other hand, when $G_4^c(r,a_0) < 0$ the critical line is preempted by a first order phase transition. On the line where $G_4^c(r,a_0) = 0$, plotted in Figs. 8(a) and 8(c), a further analysis of the expansion shows that $G_6^c(r,a_0) > 0$,

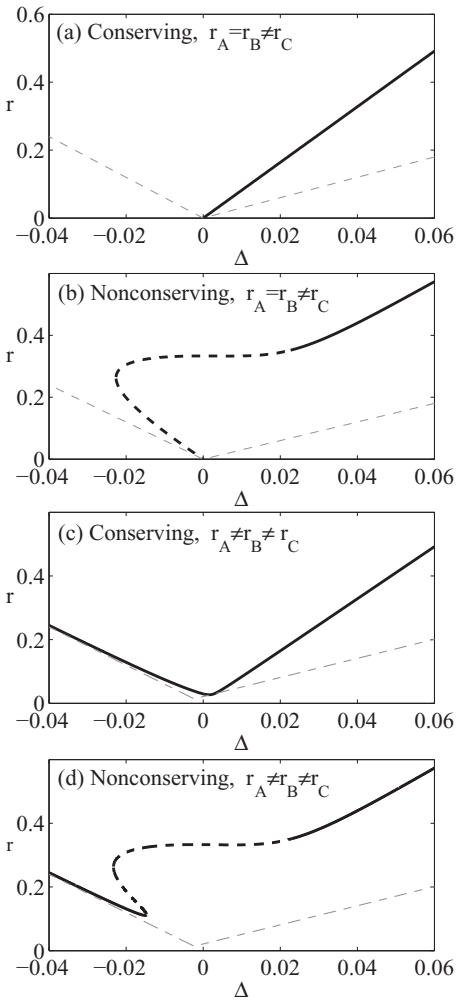

FIG. 8. Tricritical lines in the conserving and the nonconserving models. The dashed and solid thick lines represent points where $G_6 < 0$ and $G_6 > 0$, respectively. In the latter case the tricritical points are preempted by a CEP. The thin dashed gray lines denote the smallest possible values of r. The case of two equal densities, $r_A = r_B = r/3 - \Delta$ and $r_C = r/3 + 2\Delta$ or, equivalently, $a_0 = \Delta\sqrt{3}e^{i\pi/3}$, is shown in (a) and (b). Panels (c) and (d) show the fully nonequal-densities case, where $r_A = r/3 - \Delta + 0.007$, $r_B = r/3 - \Delta + 0.007$, and $r_C = r/3 + 2\Delta$.

which implies that the second order and first order transition lines join in the conserving model at a tricritical point.

In the nonconserving model the additional term in the dynamics of $\boldsymbol{\rho}(x,\tau)$ affects directly only the equation of b_m. Since this term scales as pL^2, it is negligible in comparison to the diffusive term in Eq. (A4), $-4\pi^2 m^2 b_m$, for $m \neq 0$. For $m = 0$ the nonconserving term yields the following equation:

$$\begin{aligned}\partial_\tau b_0 &= 3pL^2 \int_0^1 dx \left(\rho_0^3 - e^{-3\beta\mu}\rho_A\rho_B\rho_C\right) \\ &= 3pL^2 \left\{(1-b_0)^3 - e^{-3\beta\mu}\left[\frac{b_0^3}{27} - \frac{b_0}{3}\sum_{m_1} a_{m_1}a^\star_{m_1} \right.\right. \\ &\left.\left. + \frac{1}{3\sqrt{3}}\sum_{m_1,m_2}(a_{m_1}a_{m_2}a_{-m_1-m_2} + \text{c.c.})\right]\right\}. \qquad \text{(A14)}\end{aligned}$$

It is useful to consider the fluctuations in the overall density, denoted by δr, such that $b_0 = r + \delta r$ and r is given by Eq. (26). The parameter δr enters the equation of a_m in the following form:

$$\begin{aligned}\partial_\tau a_m = -\frac{2\pi m}{3}\Bigg[&(6\pi m - \sqrt{3}\beta r)a_m - \sqrt{3}\beta\delta r a_m \\ &+ 3\beta\sum_{m'=-\infty}^{\infty} a^\star_{-m-m'}a^\star_{m'}\Bigg]. \qquad \text{(A15)}\end{aligned}$$

In the steady state, Eq. (A14) is shown below to yield to leading order $\delta r = O(|a_m|^2, a_m a_{-m})$. As a result, the fluctuation in the density, δr, do not affect the linear stability of a_m and thus the critical line of the nonconserving model is identical to that of the conserving model.

The type of transition observed on the critical line is determined by the higher order terms in the expansion. For convenience the expansion is expressed below in terms of the steady-state density, r, instead of μ. Inserting the definition for φ in Eq. (A10) into Eq. (A14) yields to leading order

$$\delta r = \frac{6(1-r)(r^2 - 12|a_0|^2)(r + \sqrt{r^2 - 12|a_0|^2})}{r^2 - 3(1+2r)|a_0|^2}|\varphi|^2. \qquad \text{(A16)}$$

The $O(\varphi^4)$ term in the expansion of Eq. (A15) is then obtained by inserting the leading order term of a_2 in Eq. (A11) and of δr in Eq. (A16) into Eq. (A15), yielding

$$0 = 4\pi^2\delta\varphi + G_4^{nc}(r,a_0)\varphi|\varphi|^2 + O(\varphi|\varphi|^4), \qquad \text{(A17)}$$

where

$$\begin{aligned}G_4^{nc}(r,a_0) &= G_4^c(r,a_0) - \frac{1}{\varphi|\varphi|^2}\sqrt{3}\beta\delta r\, v_+^L \begin{pmatrix} a_1 \\ -a^\star_{-1}\end{pmatrix} \\ &= G_4^c(r,a_0) - \frac{24\pi^2 r(1-r)(r+\sqrt{r^2-12|a_0|^2})}{r^2 - 3(1+2r)|a_0|^2}. \qquad \text{(A18)}\end{aligned}$$

In the equal-densities case the tricritical point is found at $r = 1/3$, $G_4^{nc}(1/3,0) = 0$, as previously found in [29]. For $a_0 \neq 0$, by continuing the expansion described above it can be shown that $G_6^{nc}(r,0) < 0$ on the tricritical line for values of $|a_0|$ that are relatively small. In this case, the tricritical point is preempted by a CEP, which connects the first and second order transition line, as demonstrated in Fig. 3(b). Figures 8(b) and 8(d) show the tricritical line of the nonconserving model, defined by $\beta = \beta_c$ and $G_4^{nc}(r,a_0) = 0$, in a specific cross section of parameter space. The dashed and solid lines denote regions where $G_6^{nc}(r,a_0) < 0$ and $G_6^{nc}(r,a_0) > 0$ on the tricritical line, respectively.

APPENDIX B: DERIVATION OF HAMILTON'S EQUATIONS FOR THE NONCONSERVING ABC MODEL WITH $p = \phi L^{-2}$

In Sec. IV B the nonconserving ABC model is analyzed in the limit where $p = \phi L^{-2}$ using the macroscopic fluctuation theorem. In this appendix we derive a set of equations for the instanton trajectory that minimizes the action of the model. The trajectory is defined in terms of fields that can be regarded as the momenta conjugate to the conserving and nonconserving particles currents. In this respect, the equations derived below play the role of Hamilton's equations.

In the Lagrangian formulation presented in Sec. IV B, the instanton path is defined by the currents $\mathbf{j}(x,\tau)$ and $k(x,\tau)$ and the corresponding action is given by

$$\mathcal{I} = \int_0^T d\tau \int_0^1 dx [\mathcal{L}_c(\boldsymbol{\rho}(x,\tau),\mathbf{j}(x,\tau)) + \phi \mathcal{L}_{nc}(\boldsymbol{\rho}(x,\tau),k(x,\tau))]. \tag{B1}$$

Here the conserving and the nonconserving Lagrangian densities are given by

$$\mathcal{L}_c(\mathbf{j},\boldsymbol{\rho}) = [\mathbf{j} + \partial_x \boldsymbol{\rho} + \boldsymbol{\chi}(\boldsymbol{\rho})]\, \Sigma^{-1}(\boldsymbol{\rho})\, [\mathbf{j} + \partial_x \boldsymbol{\rho} + \boldsymbol{\chi}(\boldsymbol{\rho})]\,, \tag{B2}$$

and

$$\mathcal{L}_{nc}(\boldsymbol{\rho},k) = \mathcal{C}(\boldsymbol{\rho}) + \mathcal{A}(\boldsymbol{\rho}) - \sqrt{k^2 + 4\mathcal{A}(\boldsymbol{\rho})\mathcal{C}(\boldsymbol{\rho})} + k \ln\left[\frac{\sqrt{k^2 + 4\mathcal{A}(\boldsymbol{\rho})\mathcal{C}(\boldsymbol{\rho})} + k}{2\mathcal{C}(\boldsymbol{\rho})}\right], \tag{B3}$$

respectively. The density profile of the particles along this path is given by the continuity equation

$$\partial_\tau \boldsymbol{\rho}(x,\tau) = -\partial_x \mathbf{j}(x,\tau) + \phi \mathbf{u} k(x,\tau), \tag{B4}$$

where $\mathbf{u} = (1,1,1)^T$. In the derivation below we consider a general form of $\boldsymbol{\chi}(\boldsymbol{\rho})$, $\mathcal{A}(\boldsymbol{\rho})$, and $\mathcal{C}(\boldsymbol{\rho})$. The specific expressions of these functionals are discussed in Sec. IV B.

As mentioned in Sec. IV B, it is convenient to express the instanton path using the fields $\mathbf{H}(x,\tau)$ and $G(x,\tau)$, defined by the following equations:

$$\Sigma(\boldsymbol{\rho})\partial_x \mathbf{H} = \mathbf{j} + \partial_x \boldsymbol{\rho} + \boldsymbol{\chi}(\boldsymbol{\rho}), \tag{B5}$$

$$k = \mathcal{C}(\boldsymbol{\rho}) e^{G} - \mathcal{A}(\boldsymbol{\rho}) e^{-G}. \tag{B6}$$

In terms of these fields the Lagrangian densities are given by

$$\mathcal{L}_c(\boldsymbol{\rho},H) = \tfrac{1}{2}(\partial_x \mathbf{H})^T \Sigma(\boldsymbol{\rho})\, \partial_x \mathbf{H}, \tag{B7}$$

$$\mathcal{L}_{nc}(\boldsymbol{\rho},H) = \mathcal{C}(\boldsymbol{\rho})(1 - e^{G} + G e^{G}) + \mathcal{A}(\boldsymbol{\rho})(1 - e^{-G} - G e^{-G}), \tag{B8}$$

and the continuity equations are given by

$$\partial_\tau \boldsymbol{\rho} = -\partial_x [\Sigma(\boldsymbol{\rho})\partial_x \mathbf{H} - \partial_x \boldsymbol{\rho} - \boldsymbol{\chi}(\boldsymbol{\rho})] + \phi \mathbf{u}[C(\boldsymbol{\rho}) e^{G} - A(\boldsymbol{\rho}) e^{-G}]. \tag{B9}$$

In Eqs. (B5)–(B9) and in the derivation below the (x,τ) dependence is omitted in some cases in order to keep the notation compact.

We denote by $\bar{\mathbf{H}}$ and $\bar{G}$ the path that minimizes $\mathcal{I}$ and consider small deviations around this path defined as

$$\begin{aligned} \mathbf{H}(x,\tau) &= \bar{\mathbf{H}}(x,\tau) + \boldsymbol{\delta}_H(x,\tau), \\ G(x,\tau) &= \bar{G}(x,\tau) + \delta_G(x,\tau). \end{aligned} \tag{B10}$$

Similarly using the continuity equations one can define the fluctuation of the density profile around the optimal path, as

$$\boldsymbol{\rho}(x,\tau) = \bar{\boldsymbol{\rho}}(x,\tau) + \boldsymbol{\delta}_\rho(x,\tau), \tag{B11}$$

where $\bar{\boldsymbol{\rho}}$ is obtained by inserting $\bar{\mathbf{H}}$ and $\bar{G}$ into Eq. (B9). The bar notation here should not be confused with that used in Sec. IV B to denote the density profile at the end of the instanton path.

Below we derive the first order correction to the action due to $\boldsymbol{\delta}_H$ and δ_G, defined as

$$\mathcal{I} = \int_0^T d\tau \int_0^1 dx \big[\mathcal{L}_c(\bar{\boldsymbol{\rho}},\bar{\mathbf{H}}) + \mathcal{L}_{nc}(\bar{\boldsymbol{\rho}},\bar{G}) + \delta\mathcal{L}^{(1)} + O\big(\delta_{H,\alpha}^2,\delta_G^2\big)\big]. \tag{B12}$$

The optimal trajectory is defined by the equation $\delta\mathcal{L}^{(1)} = 0$. As shown below, it is, in fact, more convenient to express this equation in terms of the fields $\boldsymbol{\delta}_\rho$ and δ_G.

The simpler part in the first order expansion of $\mathcal{I}$ is the expansion of the nonconserving Lagrangian density in terms of δ_G and $\boldsymbol{\delta}_\rho$. Inserting Eqs. (B10) and (B11) into the form of $\mathcal{L}_{nc}$ yields the following expansion:

$$\begin{aligned} \delta\mathcal{L}_{nc}(\boldsymbol{\rho},G) &= \mathcal{L}_{nc}(\boldsymbol{\rho},G) - \mathcal{L}_{nc}(\bar{\boldsymbol{\rho}},\bar{G}) \\ &= \sum_\alpha \delta_{\rho,\alpha}[\partial_{\rho_\alpha}\mathcal{C}(\bar{\boldsymbol{\rho}})(1 - e^{\bar{G}} + \bar{G}e^{\bar{G}}) \\ &\quad + \partial_{\rho_\alpha}\mathcal{A}(\bar{\boldsymbol{\rho}})(1 - e^{-\bar{G}} - \bar{G}e^{-\bar{G}})] \\ &\quad + \phi\delta_G[\mathcal{C}(\bar{\boldsymbol{\rho}})\bar{G}e^{\bar{G}} + \mathcal{A}(\bar{\boldsymbol{\rho}})\bar{G}e^{-\bar{G}}] + O\big(\delta_{\rho,\alpha}^2,\delta_G^2\big). \end{aligned} \tag{B13}$$

The conserving Lagrangian density should be expanded first in terms of $\boldsymbol{\delta}_H$ and $\boldsymbol{\delta}_\rho$, yielding

$$\begin{aligned} \delta\mathcal{L}_c(\boldsymbol{\rho},\mathbf{H}) &= \frac{1}{2}(\partial_x \mathbf{H})^T \Sigma(\boldsymbol{\rho})\, \partial_x \mathbf{H} - \mathcal{L}_c(\bar{\boldsymbol{\rho}},\bar{\mathbf{H}}) \\ &= \partial_x \bar{\mathbf{H}}^T \Sigma(\bar{\boldsymbol{\rho}})\partial_x \boldsymbol{\delta}_H + \frac{1}{2}\sum_\alpha \delta_{\rho,\alpha}(\partial_x \bar{\mathbf{H}})^T \partial_{\rho_\alpha}\Sigma(\bar{\boldsymbol{\rho}})\partial_x \bar{\mathbf{H}}. \end{aligned} \tag{B14}$$

The first term in the line above can be further simplified by employing integration by parts over x of this term, yielding

$$\begin{aligned} K &\equiv \int_0^T d\tau \int_0^1 dx\, \partial_x \bar{\mathbf{H}}^T \Sigma(\bar{\boldsymbol{\rho}})\partial_x \boldsymbol{\delta}_H \\ &= -\int_0^T d\tau \int_0^1 dx\, \bar{\mathbf{H}}^T \partial_x [\Sigma(\bar{\boldsymbol{\rho}})\partial_x \boldsymbol{\delta}_H]. \end{aligned} \tag{B15}$$

Here and below the boundary terms of the integration by parts over x vanish due to the periodic boundary condition.

As mentioned above, it is convenient to express the terms in $\delta\mathcal{L}^{(1)}$ that involve $\boldsymbol{\delta}_H$ in terms of the fields $\boldsymbol{\delta}_\rho$ and δ_G. This can be done by inserting Eqs. (B10) and (B11) into the continuity equation (B9), yielding

$$\begin{aligned}\partial_x[\Sigma(\bar{\boldsymbol{\rho}})\partial_x\delta_H]_\alpha = &-\partial_\tau\delta_{\rho,\alpha}+\partial_x^2\delta_{\rho,\alpha}\\ &+\sum_{\alpha'}\partial_x\left\{\delta_{\rho,\alpha'}\left[\partial_{\rho_{\alpha'}}\Sigma(\bar{\boldsymbol{\rho}})\partial_x\,\bar{\mathbf{H}}\right]_\alpha\right.\\ &\left.+\delta_{\rho,\alpha'}\partial_{\rho_{\alpha'}}\chi_\alpha(\bar{\boldsymbol{\rho}})\right\}\\ &+\phi\delta_G[C(\bar{\boldsymbol{\rho}})e^{\bar{G}}+A(\bar{\boldsymbol{\rho}})e^{-\bar{G}}]. \quad \text{(B16)}\end{aligned}$$

Inserting this expression into Eq. (B15) yields an integral which involves derivatives of $\boldsymbol{\delta}_\rho$ and δ_G. We wish, however, to obtain an expression of $\delta\mathcal{L}^{(1)}$ which involves only local terms of the variational fields. This can be done using the proper integrations by parts over x and τ, which yield

$$\begin{aligned}K=\int_0^T d\tau\int_0^1 dx\sum_\alpha\left\{\delta_{\rho,\alpha}\left[-\partial_\tau\bar{H}_\alpha-\partial_x\bar{\mathbf{H}}^T\partial_{\rho_\alpha}\Sigma(\bar{\boldsymbol{\rho}})\partial_x\bar{\mathbf{H}}\right.\right.\\ \left.-\partial_x^2\bar{H}_{\rho,\alpha}-\partial_x\bar{\mathbf{H}}^T\partial_{\rho_\alpha}\boldsymbol{\chi}(\bar{\boldsymbol{\rho}})\right]\\ \left.-\phi\delta_G\bar{H}_\alpha[C(\bar{\boldsymbol{\rho}})e^{\bar{G}}+A(\bar{\boldsymbol{\rho}})e^{-\bar{G}}]\right\}+O\left(\delta_{\rho,\alpha}^2,\delta_G^2\right). \quad \text{(B17)}\end{aligned}$$

Finally, by inserting Eqs. (B13)–(B17) into Eq. (B12) one obtains the following expression for the first order term in the expansion of the action:

$$\begin{aligned}\delta\mathcal{L}^{(1)}=\sum_\alpha\delta_{\rho,\alpha}\left[-\partial_\tau\bar{H}_\alpha-\frac{1}{2}\partial_x\bar{\mathbf{H}}^T\partial_{\rho_\alpha}\Sigma(\bar{\boldsymbol{\rho}})\partial_x\bar{\mathbf{H}}\right.\\ \left.-\partial_x^2\bar{H}_{\rho,\alpha}-\partial_x\bar{\mathbf{H}}^T\partial_{\rho_\alpha}\boldsymbol{\chi}(\bar{\boldsymbol{\rho}})\right]-\phi\delta_G\left(\bar{G}-\sum_\alpha\bar{H}_\alpha\right)\\ \times[C(\bar{\boldsymbol{\rho}})e^{\bar{G}}+A(\bar{\boldsymbol{\rho}})e^{-\bar{G}}]. \quad \text{(B18)}\end{aligned}$$

The solution for $\delta\mathcal{L}^{(1)}=0$ corresponds to the extremum of the action, which is therefore given by

$$\bar{G}=\bar{H}_A+\bar{H}_B+\bar{H}_C \quad \text{(B19)}$$

$$\begin{aligned}\partial_\tau\bar{H}_\alpha=&-\partial_x^2\bar{\mathbf{H}}^T+\partial_{\rho_\alpha}\boldsymbol{\chi}(\bar{\boldsymbol{\rho}})\partial_x\bar{H}_\alpha-\tfrac{1}{2}(\partial_x\bar{\mathbf{H}})^T\partial_{\rho_\alpha}\Sigma(\bar{\boldsymbol{\rho}})\,\partial_x\bar{\mathbf{H}}\\ &+\phi[\partial_{\rho_\alpha}\mathcal{C}(\bar{\boldsymbol{\rho}})(1-e^{\bar{G}})+\partial_{\rho_\alpha}\mathcal{A}(\bar{\boldsymbol{\rho}})(1-e^{-\bar{G}})]. \quad \text{(B20)}\end{aligned}$$

The instanton path is fully described by the two equations above and the definition of $\bar{\boldsymbol{\rho}}$, given by

$$\begin{aligned}\partial_\tau\bar{\boldsymbol{\rho}}=&-\partial_x[\Sigma(\bar{\boldsymbol{\rho}})\partial_x\bar{\mathbf{H}}-\partial_x\bar{\boldsymbol{\rho}}-\boldsymbol{\chi}(\bar{\boldsymbol{\rho}})]\\ &+\phi\mathbf{u}[\mathcal{C}(\bar{\boldsymbol{\rho}})e^{\bar{G}}-\mathcal{A}(\bar{\boldsymbol{\rho}})e^{-\bar{G}}]. \quad \text{(B21)}\end{aligned}$$

In Sec. IV B the bar notation is omitted from the above result in order to simplify the notation.

[1] H. Spohn, J. Phys. A **16**, 4275 (1983).
[2] R. K. P. Zia and B. Schmittmann, in *Phase Transitions and Critical Phenomena*, edited by C. Domb and J. L. Lebowitz (Academic Press, London, 1995), Vol. 17.
[3] S. Lepri, R. Livi, and A. Politi, Phys. Rep. **377**, 1 (2003).
[4] B. Derrida, J. Stat. Mech. (2007) P07023.
[5] R. A. Blythe and M. R. Evans, J. Phys. A **40**, R333 (2007).
[6] A. Dhar, Adv. Phys. **57**, 457 (2008).
[7] T. Sadhu, S. N. Majumdar, and D. Mukamel, Phys. Rev. E **84**, 051136 (2011).
[8] V. A. Antonov, Vest. Liningrad Univ. **7**, 135 (1962) [translation in Symp. - Int. Astron. Union **113**, 525 (1995)].
[9] D. Lynden-Bell and R. Wood, Mon. Not. R. Astron. Soc. **138**, 495 (1968).
[10] W. Thirring, Z. Phys. A: Hadrons Nucl. **235**, 339 (1970).
[11] P. Hertel and W. Thirring, Ann. Phys. **63**, 520 (1971).
[12] D. Lynden-Bell, Physica A **263**, 293 (1999).
[13] W. Thirring, H. Narnhofer, and H. A. Posch, Phys. Rev. Lett. **91**, 130601 (2003).
[14] J. Barré, D. Mukamel, and S. Ruffo, Phys. Rev. Lett. **87**, 030601 (2001).
[15] J. Barré, D. Mukamel, and S. Ruffo, in *Dynamics and Thermodynamics of Systems with Long-Range Interactions*, edited by T. Dauxois, S. Ruffo, E. Arimondo, and M. Wilkens, Lecture Notes in Physics Vol. 602 (Springer-Verlag, New York, 2002), pp. 45–67.
[16] D. Mukamel, S. Ruffo, and N. Schreiber, Phys. Rev. Lett. **95**, 240604 (2005).
[17] R. S. Ellis, H. Touchette, and B. Turkington, Physica A **335**, 518 (2004).
[18] H. Touchette, R. S. Ellis, and B. Turkington, Physica A **340**, 138 (2004).
[19] H. Touchette and R. S. Ellis, in *Complexity, Metastability and Nonextensivity: Proceedings of the 31st Workshop of the International School of Solid State Physics*, edited by C. Beck, G. Benedek, A. Rapisarda, and C. Tsallis (World Scientific, Singapore, 2005).
[20] F. Bouchet and J. Barré, J. Stat. Phys. **118**, 1073 (2005).
[21] D. Mukamel, in *Dynamics and Thermodynamics of Systems with Long Range Interactions: Theory and Experiments*, edited by A. Campa, A. Giansanti, G. Morigi, and F. S. Labini, American Institute of Physics Conference Series Vol. 970 (AIP, New York, 2008), pp. 22–38.
[22] T. Misawa, Y. Yamaji, and M. Imada, J. Phys. Soc. Jpn. **75**, 064705 (2006).
[23] S. Großkinsky and G. M. Schütz, J. Stat. Phys. **132**, 77 (2008).
[24] A. Lederhendler and D. Mukamel, Phys. Rev. Lett. **105**, 150602 (2010).
[25] O. Cohen and D. Mukamel, Phys. Rev. Lett. **108**, 060602 (2012).
[26] M. R. Evans, Y. Kafri, H. M. Koduvely, and D. Mukamel, Phys. Rev. Lett. **80**, 425 (1998).
[27] M. R. Evans, Y. Kafri, H. M. Koduvely, and D. Mukamel, Phys. Rev. E **58**, 2764 (1998).
[28] M. Clincy, B. Derrida, and M. R. Evans, Phys. Rev. E **67**, 066115 (2003).
[29] A. Lederhendler, O. Cohen, and D. Mukamel, J. Stat. Mech: Theory Exp. (2010) P11016.
[30] O. Cohen and D. Mukamel, J. Phys. A **44**, 415004 (2011).
[31] T. Bodineau and B. Derrida, J. Stat. Phys. **145**, 745 (2011).
[32] L. Bertini and P. Buttà, J. Stat. Phys. **152**, 15 (2013).

[33] M. I. Freidlinand and A. D. Wentzell, *Random Perturbations of Dynamical Systems* (Springer-Verlag, Berlin, 1984).
[34] L. Bertini, A. De Sole, D. Gabrielli, G. Jona-Lasinio, and C. Landim, Phys. Rev. Lett. **87**, 040601 (2001).
[35] A. N. Jordan and E. V. Sukhorukov, Phys. Rev. Lett. **93**, 260604 (2004).
[36] L. Bertini, A. De Sole, D. Gabrielli, G. Jona-Lasinio, and C. Landim, Phys. Rev. Lett. **94**, 030601 (2005).
[37] J. Tailleur, J. Kurchan, and V. Lecomte, J. Phys. A **41**, 505001 (2008).
[38] H. Touchette and R. Harris, in *Nonequilibrium Statistical Physics of Small Systems: Fluctuation Relations and Beyond*, edited by R. Klages, W. Just, and C. Jarzynski (Wiley-VCH, Weinheim, 2012).
[39] M. Kac, G. E. Uhlenbeck, and P. C. Hemmer, J. Math. Phys. **4**, 216 (1963).
[40] In [29] the grand-canonical Hamiltonian was defined based on the Hamiltonian in Eq. (5). In this case one has to add a term of the form $-\frac{1}{6}N(N-1)$ from $\mathcal{H}_{GC}(\boldsymbol{\zeta})$ in order to allow for local dynamics whose rate does not depend on N. This additional term is not necessary when using the Hamiltonian in Eq. (7), since the potential landscape changes only locally when adding or removing a triplet of ABC particles. This suggests that Eq. (7) is a more natural representation of the stationary measure of the equal-densities ABC model.
[41] A. Ayyer, E. A. Carlen, J. L. Lebowitz, P. K. Mohanty, D. Mukamel, and E. R. Speer, J. Stat. Phys. **137**, 1166 (2009).
[42] O. Cohen and D. Mukamel, J. Stat. Mech. (2012) P12017.
[43] T. Bodineau, B. Derrida, V. Lecomte, and F. van Wijland, J. Stat. Phys. **133**, 1013 (2008).
[44] M. Creutz, Phys. Rev. Lett. **50**, 1411 (1983).
[45] In the algorithm described here $N_d \geqslant 0$, since the demon can only condense triplets of ABC particles if it has some in its bag. For negative $\mu(r)$ the algorithm should be modified to allow only for $N_d \leqslant 0$. This can be done by allowing the demon to store in its bag only triplets of 000.
[46] G. Jona-Lasinio, C. Landim, and M. E. Vares, Probab. Theory Rel. Fields **97**, 339 (1993).
[47] T. Bodineau and M. Lagouge, J. Stat. Phys. **139**, 201 (2010).
[48] T. Bodineau and M. Lagouge, Ann. Appl. Probab. **22**, 2282 (2012).
[49] The time-reversal symmetry of $k(x,\tau)$ is not broken in the equal-densities ABC, where $\mathcal{C}(\boldsymbol{\rho}^\star)$ and $\mathcal{A}(\boldsymbol{\rho}^\star)$, which are chosen such that they maintain detailed balance with respect to the conserving measure, are homogenous in space.